Electronic Supplementary Material (ESI) for CrystEngComm.
This journal is © The Royal Society of Chemistry 2022

Benzene and Triazine-Based Porous Organic Polymers with Azo, Azoxy and Azodioxy Linkages: A Computational Study

Petar Šutalo, Mateja Pisačić, Ivana Biljan* and Ivan Kodrin*

Supplementary Materials

Table of Contents

1. Interactions of CO_2 and N_2 with the selected organic molecules/fragments

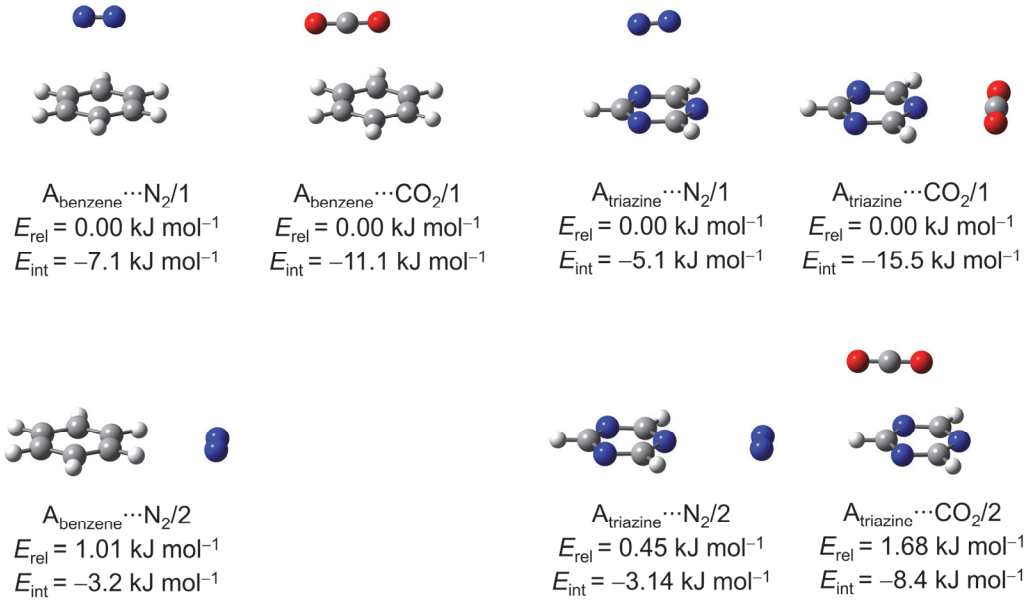

Figure S1. The B3LYP-D3(BJ)/def2-TZVP optimized geometries of the selected complexes between fragments $\mathbf{A_{benzene}}$ and $\mathbf{A_{triazine}}$ and one molecule of N_2 or CO_2. Relative energies of the selected complexes (E_{rel}) and BSSE corrected interaction energies (E_{int}).

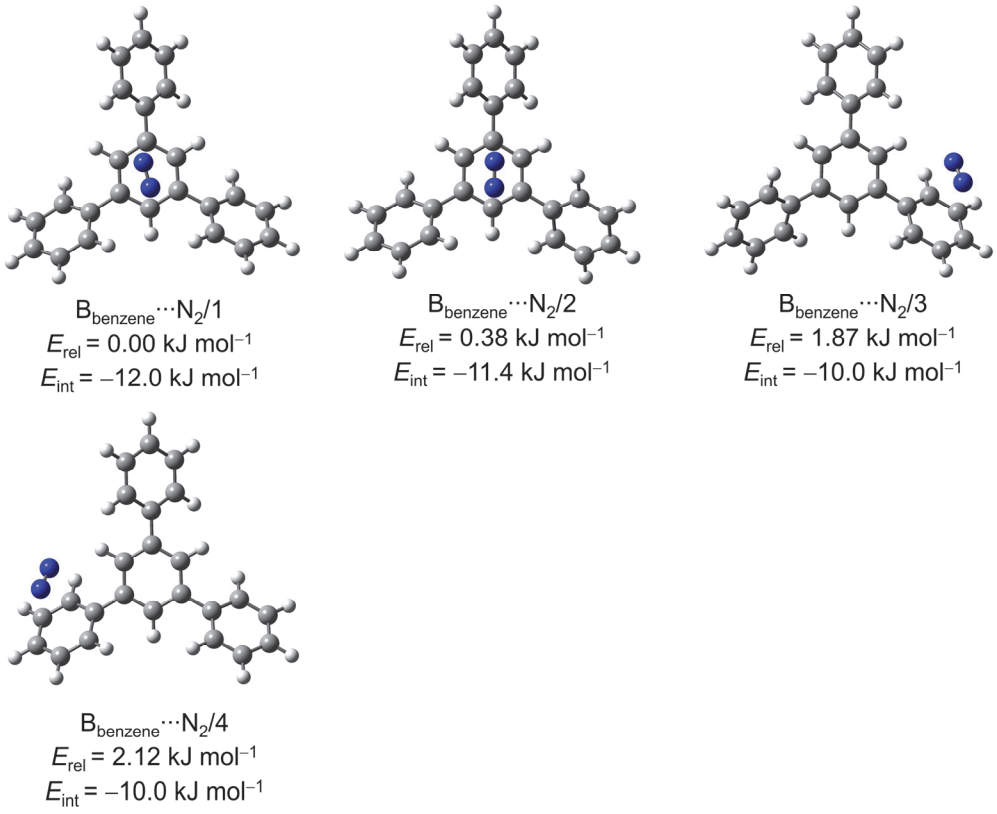

Figure S2. The B3LYP-D3(BJ)/def2-TZVP optimized geometries of the selected complexes between fragment **B$_{benzene}$** and one molecule of N_2. Relative energies of the selected complexes (E_{rel}) and BSSE corrected interaction energies (E_{int}).

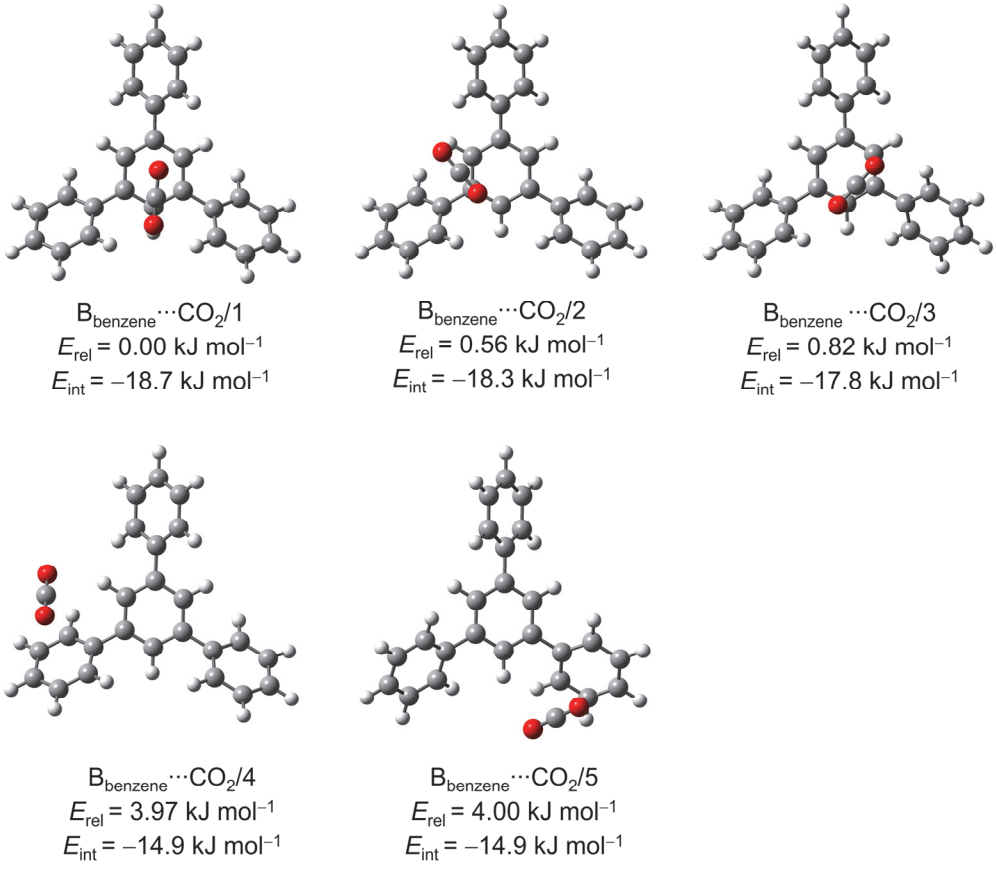

Figure S3. The B3LYP-D3(BJ)/def2-TZVP optimized geometries of the selected complexes between fragment $\mathbf{B_{benzene}}$ and one molecule of CO_2. Relative energies of the selected complexes (E_{rel}) and BSSE corrected interaction energies (E_{int}).

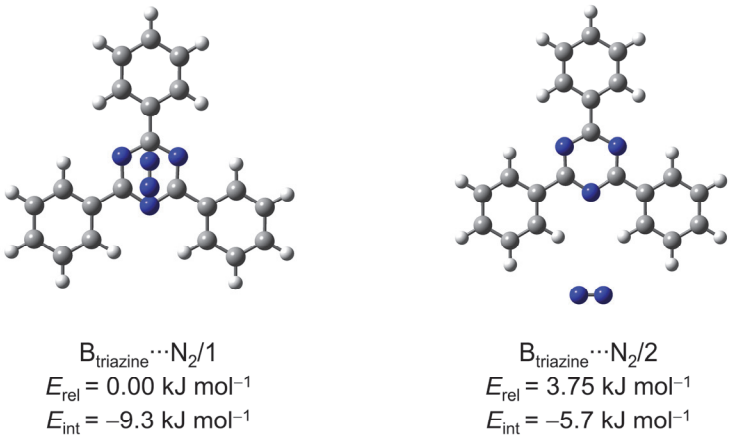

Figure S4. The B3LYP-D3(BJ)/def2-TZVP optimized geometries of the selected complexes between fragment $\mathbf{B_{triazine}}$ and one molecule of N_2. Relative energies of the selected complexes (E_{rel}) and BSSE corrected interaction energies (E_{int}).

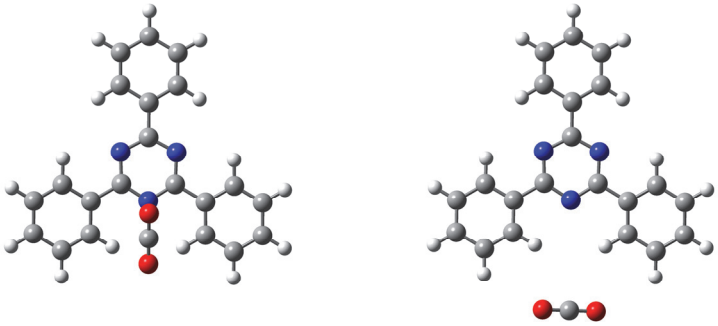

Figure S5. The B3LYP-D3(BJ)/def2-TZVP optimized geometries of the selected complexes between fragment **$B_{triazine}$** and one molecule of CO_2. Relative energies of the selected complexes (E_{rel}) and BSSE corrected interaction energies (E_{int}).

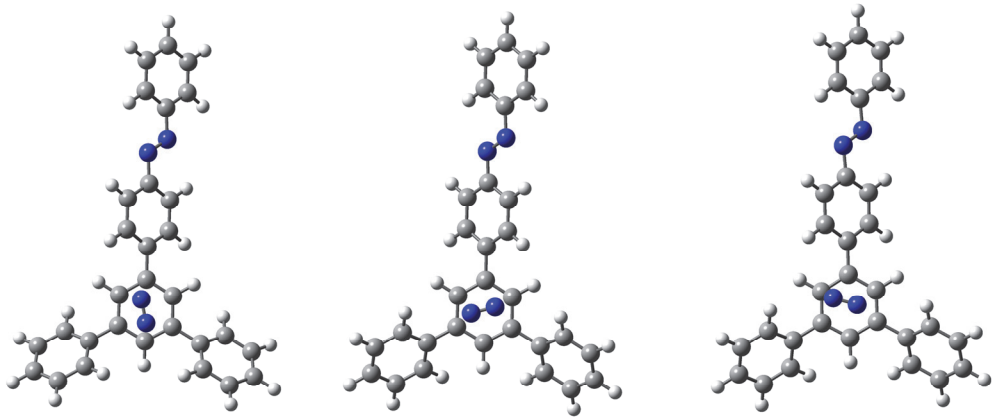

Figure S6. The B3LYP-D3(BJ)/def2-TZVP optimized geometries of the selected complexes between fragment **1C** and one molecule of N_2. Relative energies of the selected complexes (E_{rel}) and BSSE corrected interaction energies (E_{int}).

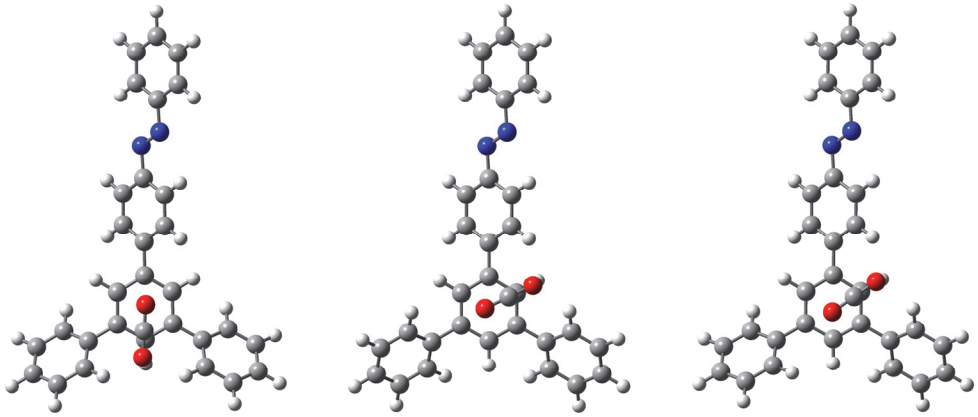

Figure S7. The B3LYP-D3(BJ)/def2-TZVP optimized geometries of the selected complexes between fragment **1C** and one molecule of CO_2. Relative energies of the selected complexes (E_{rel}) and BSSE corrected interaction energies (E_{int}).

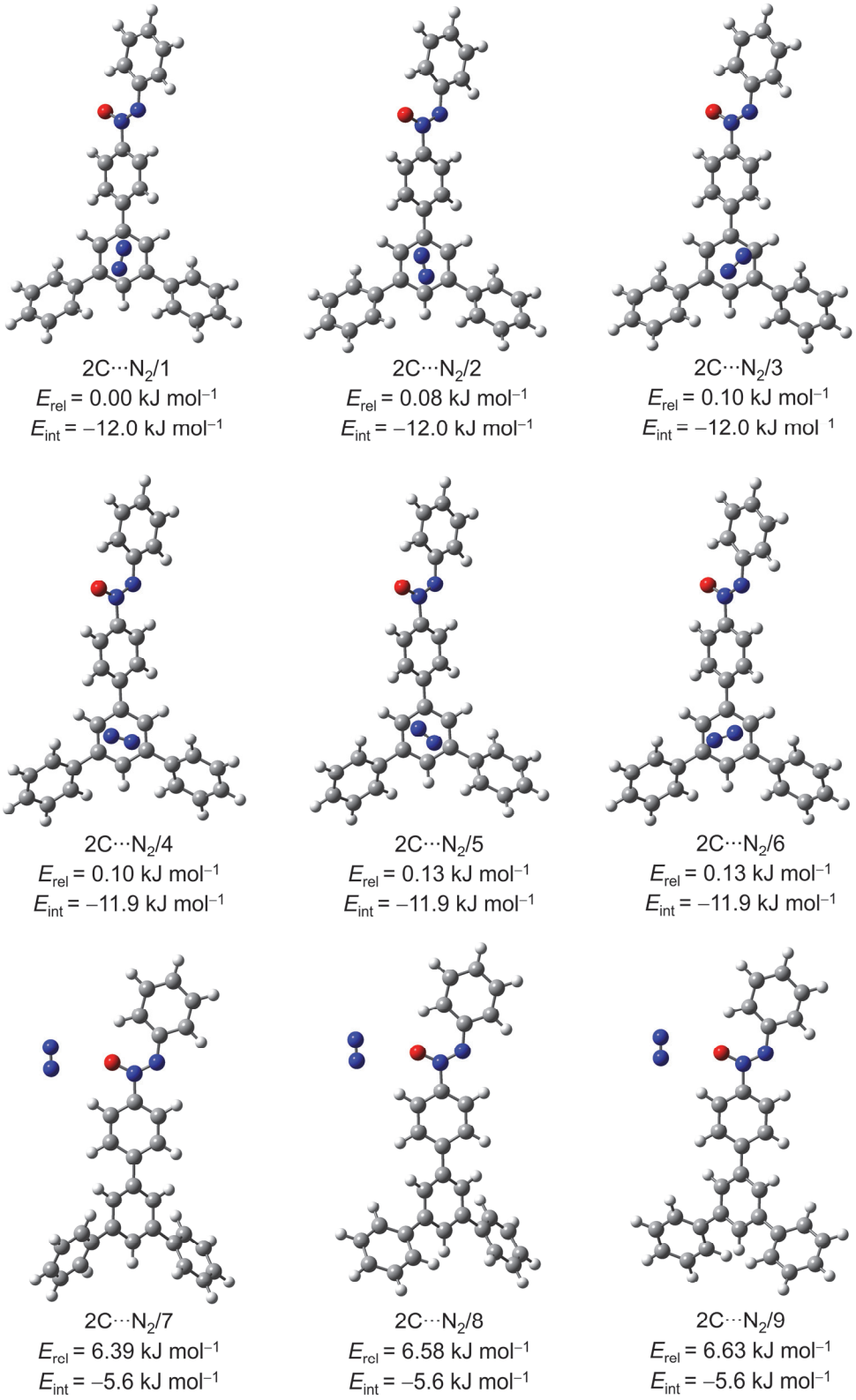

Figure S8. The B3LYP-D3(BJ)/def2-TZVP optimized geometries of the selected complexes between fragment **2C** and one molecule of N_2. Relative energies of the selected complexes (E_{rel}) and BSSE corrected interaction energies (E_{int}).

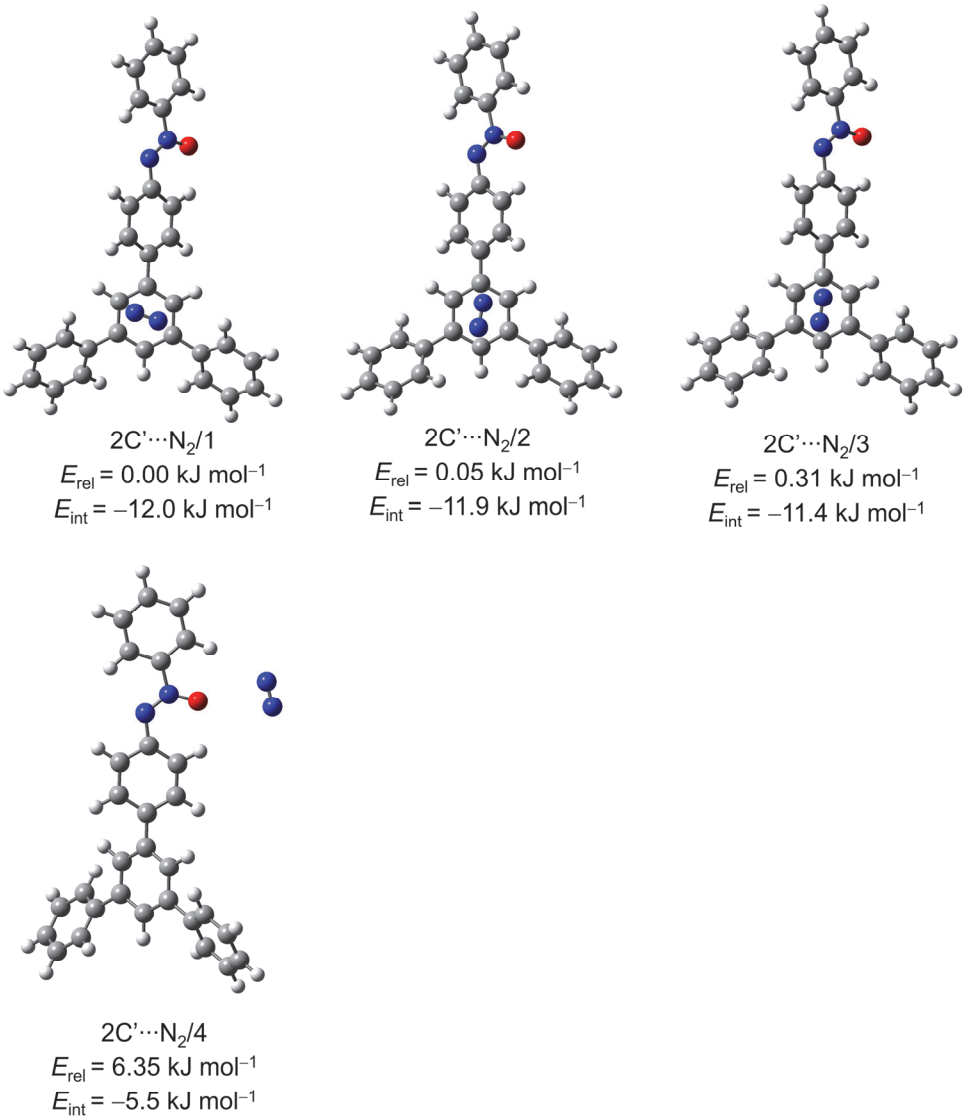

Figure S9. The B3LYP-D3(BJ)/def2-TZVP optimized geometries of the selected complexes between fragment **2C'** and one molecule of N_2. Relative energies of the selected complexes (E_{rel}) and BSSE corrected interaction energies (E_{int}).

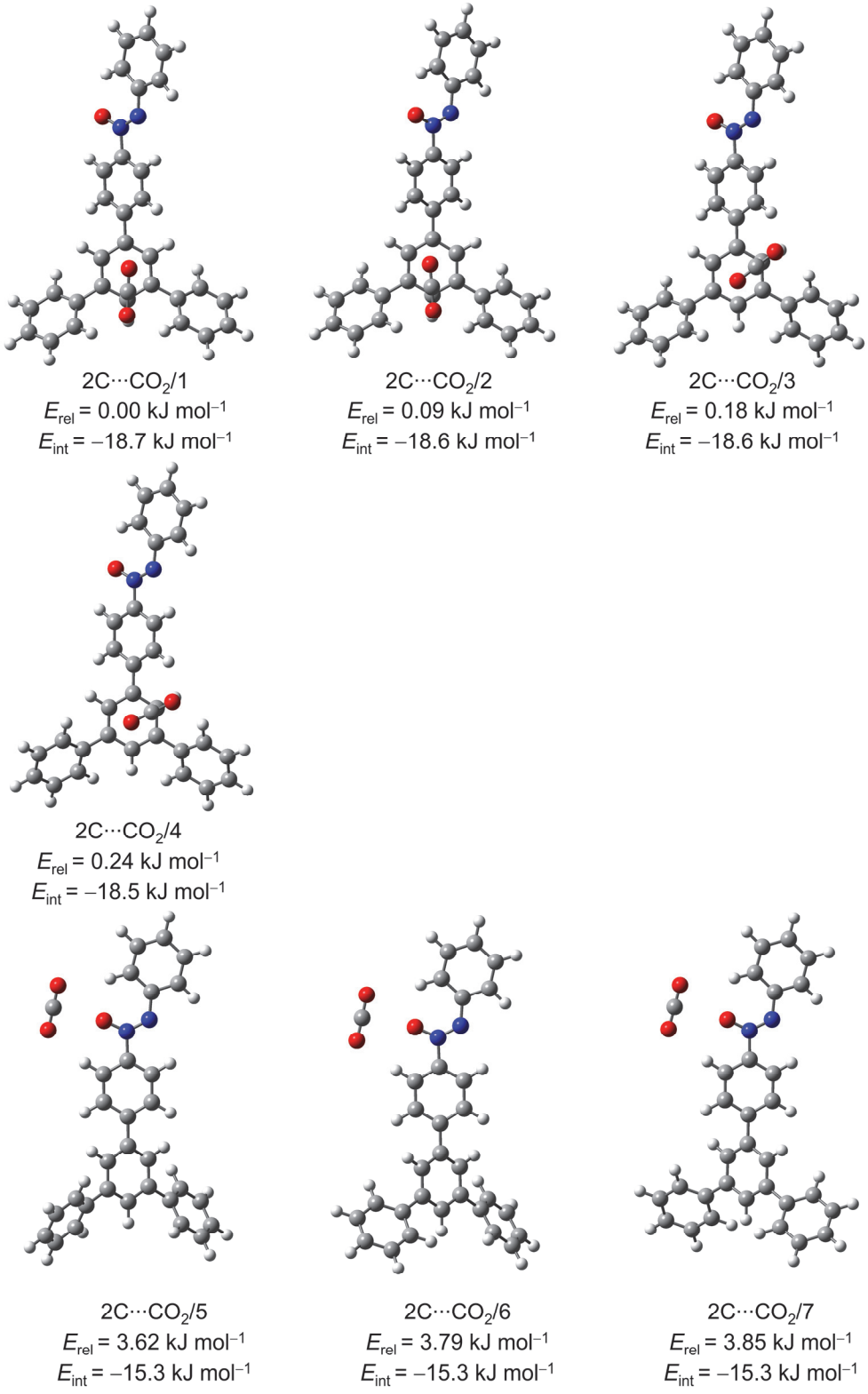

Figure S10. The B3LYP-D3(BJ)/def2-TZVP optimized geometries of the selected complexes between fragment **2C** and one molecule of CO_2. Relative energies of the selected complexes (E_{rel}) and BSSE corrected interaction energies (E_{int}).

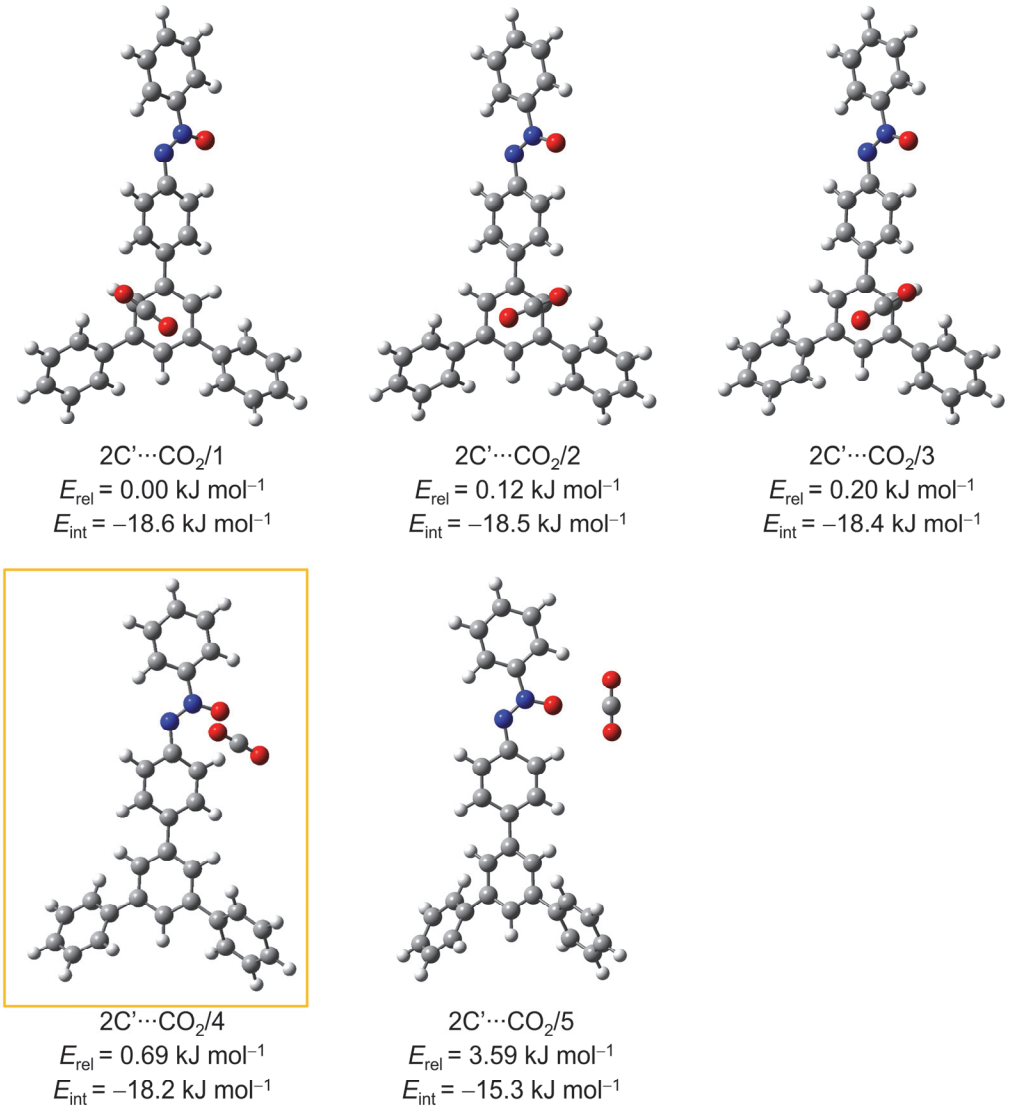

Figure S11. The B3LYP-D3(BJ)/def2-TZVP optimized geometries of the selected complexes between fragment **2C'** and one molecule of CO_2. Relative energies of the selected complexes (E_{rel}) and BSSE corrected interaction energies (E_{int}).

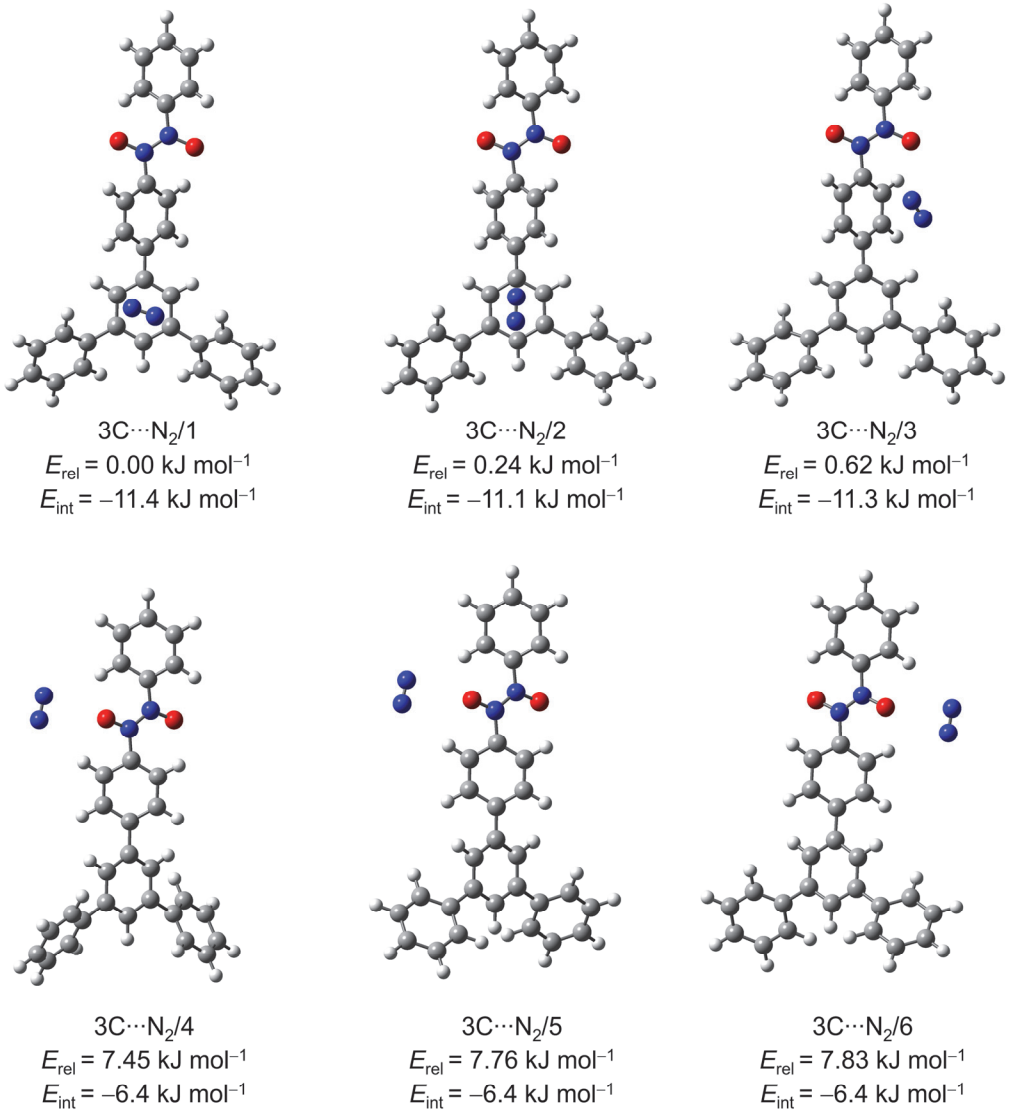

Figure S12. The B3LYP-D3(BJ)/def2-TZVP optimized geometries of the selected complexes between fragment **3C** and one molecule of N_2. Relative energies of the selected complexes (E_{rel}) and BSSE corrected interaction energies (E_{int}).

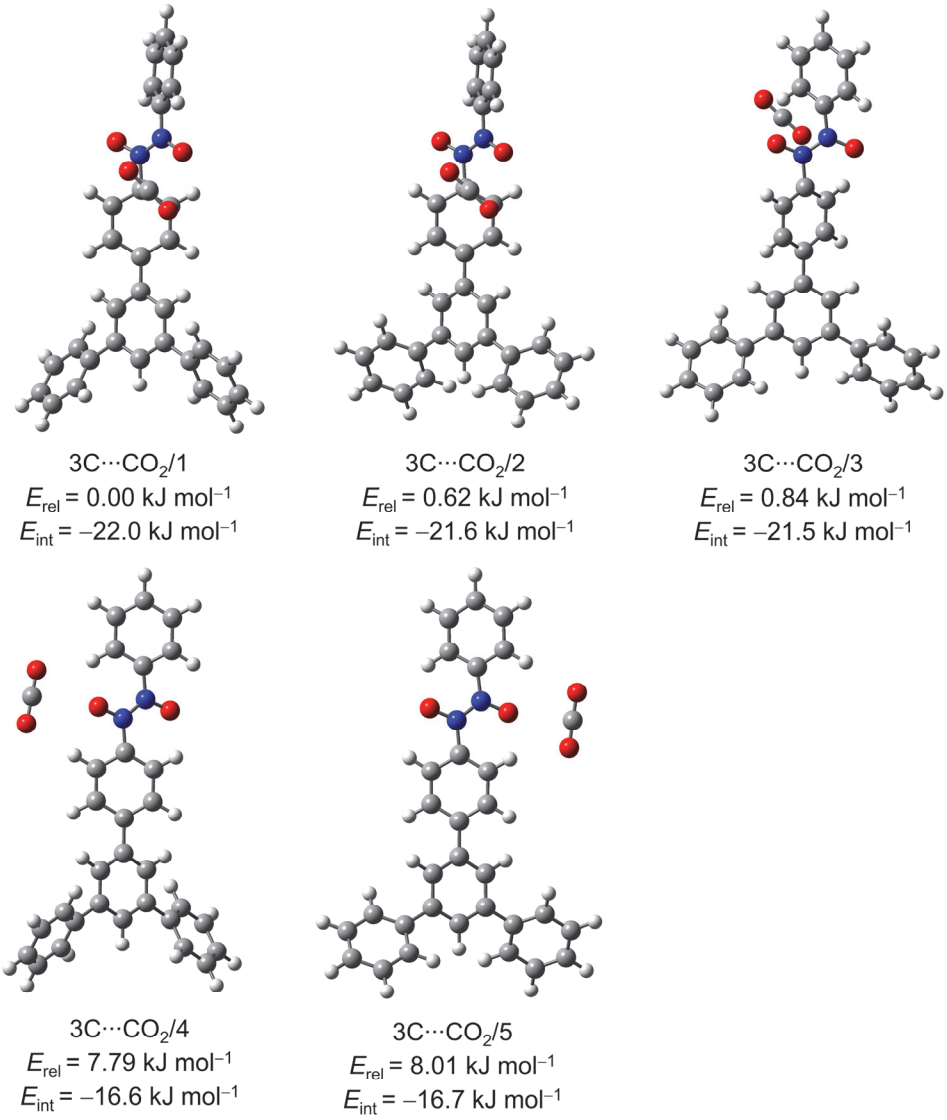

Figure S13. The B3LYP-D3(BJ)/def2-TZVP optimized geometries of the selected complexes between fragment **3C** and one molecule of CO_2. Relative energies of the selected complexes (E_{rel}) and BSSE corrected interaction energies (E_{int}).

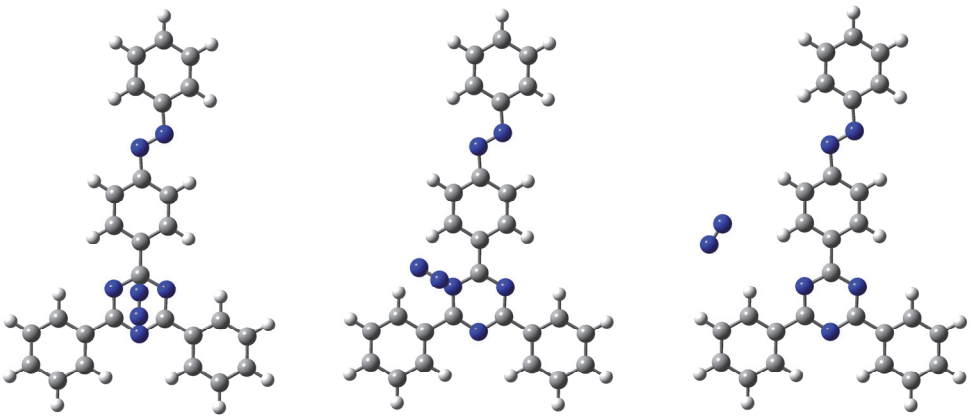

Figure S14. The B3LYP-D3(BJ)/def2-TZVP optimized geometries of the selected complexes between fragment **4C** and one molecule of N_2. Relative energies of the selected complexes (E_{rel}) and BSSE corrected interaction energies (E_{int}).

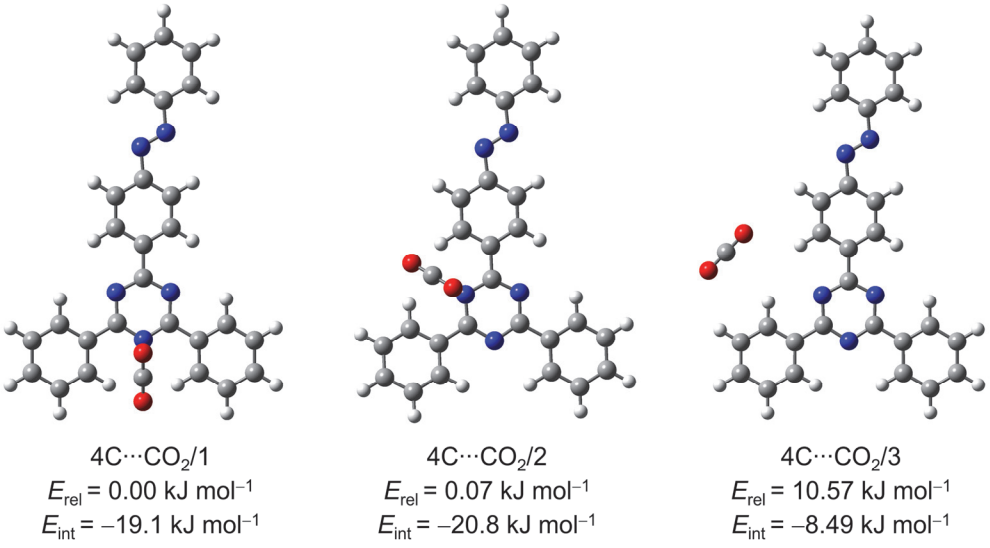

Figure S15. The B3LYP-D3(BJ)/def2-TZVP optimized geometries of the selected complexes between fragment **4C** and one molecule of CO_2. Relative energies of the selected complexes (E_{rel}) and BSSE corrected interaction energies (E_{int}).

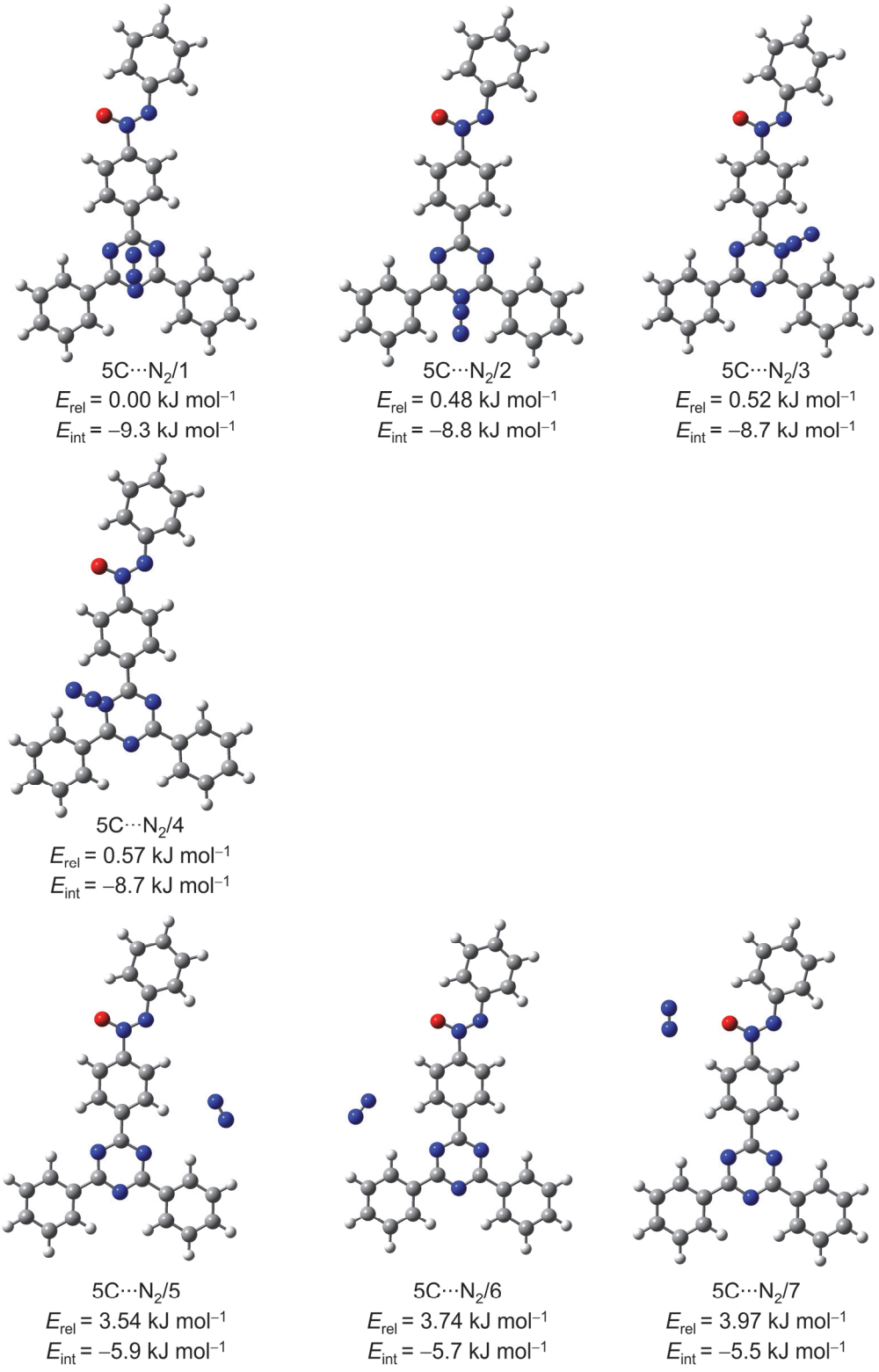

Figure S16. The B3LYP-D3(BJ)/def2-TZVP optimized geometries of the selected complexes between fragment **5C** and one molecule of N_2. Relative energies of the selected complexes (E_{rel}) and BSSE corrected interaction energies (E_{int}).

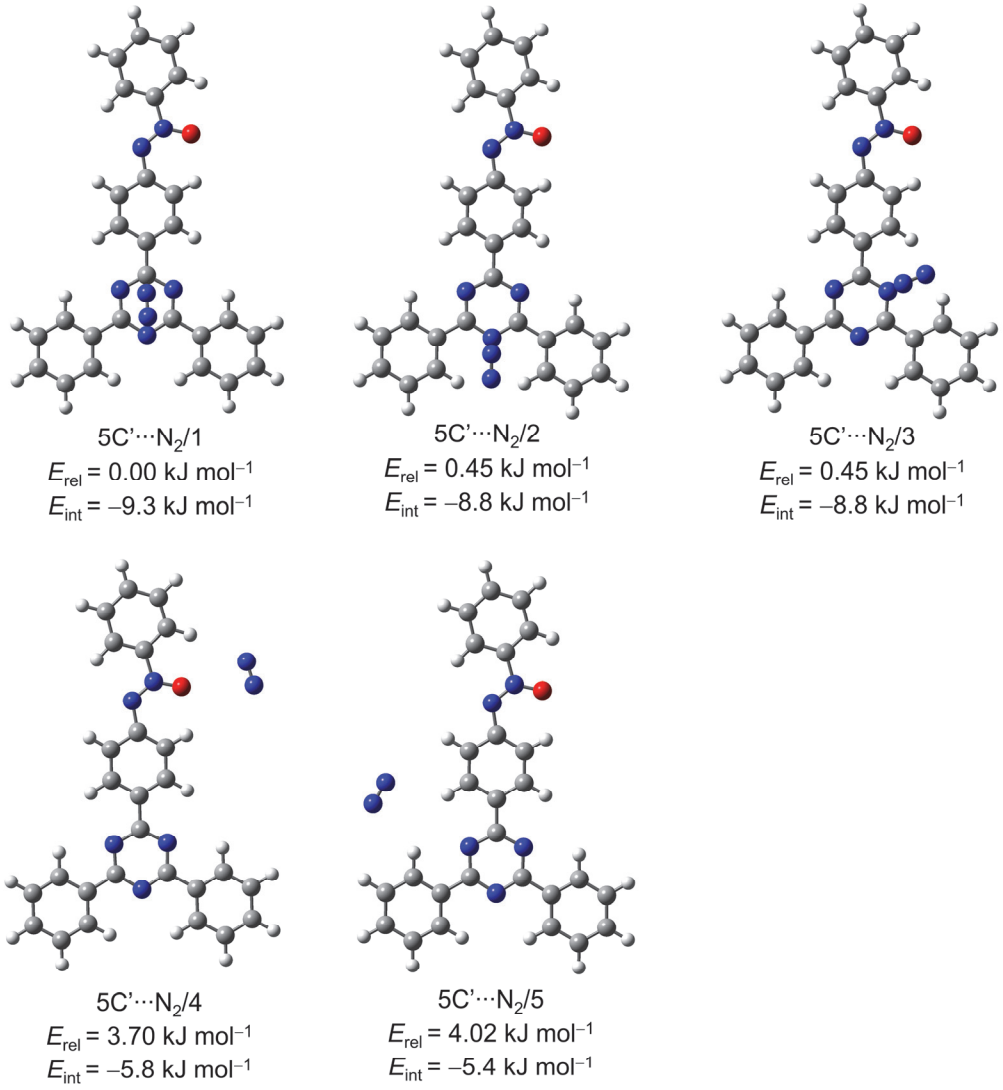

Figure S17. The B3LYP-D3(BJ)/def2-TZVP optimized geometries of the selected complexes between fragment **5C'** and one molecule of N_2. Relative energies of the selected complexes (E_{rel}) and BSSE corrected interaction energies (E_{int}).

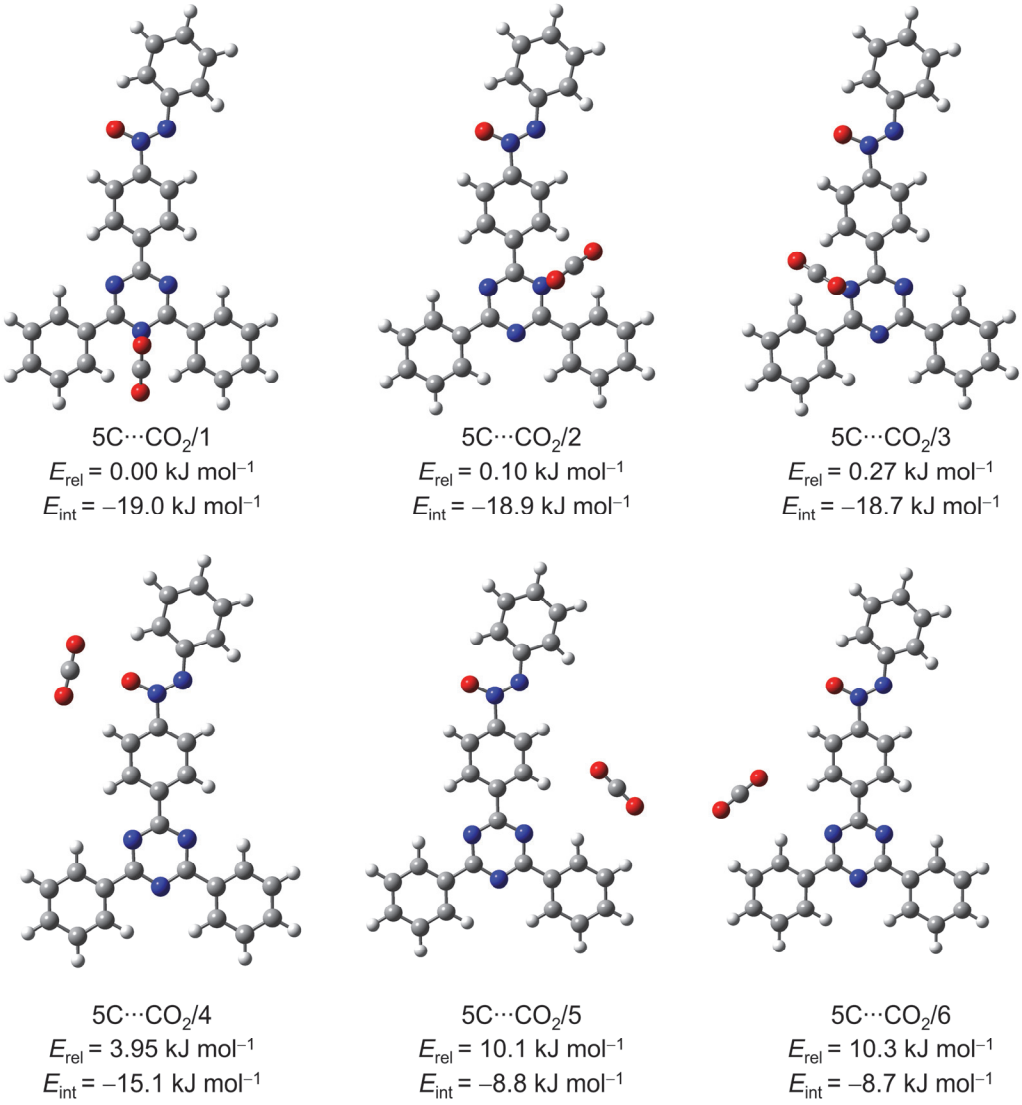

Figure S18. The B3LYP-D3(BJ)/def2-TZVP optimized geometries of the selected complexes between fragment **5C** and one molecule of CO_2. Relative energies of the selected complexes (E_{rel}) and BSSE corrected interaction energies (E_{int}).

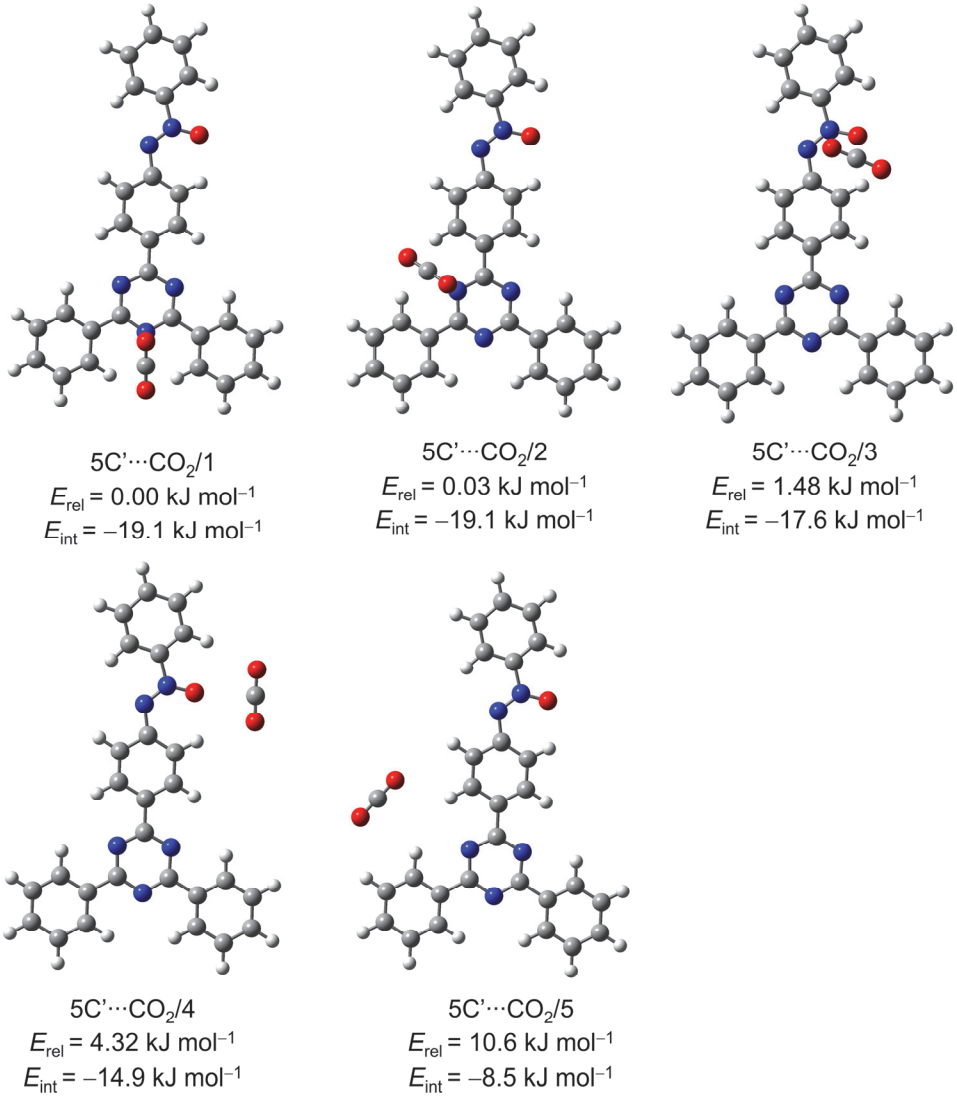

Figure S19. The B3LYP-D3(BJ)/def2-TZVP optimized geometries of the selected complexes between fragment **5C'** and one molecule of CO_2. Relative energies of the selected complexes (E_{rel}) and BSSE corrected interaction energies (E_{int}).

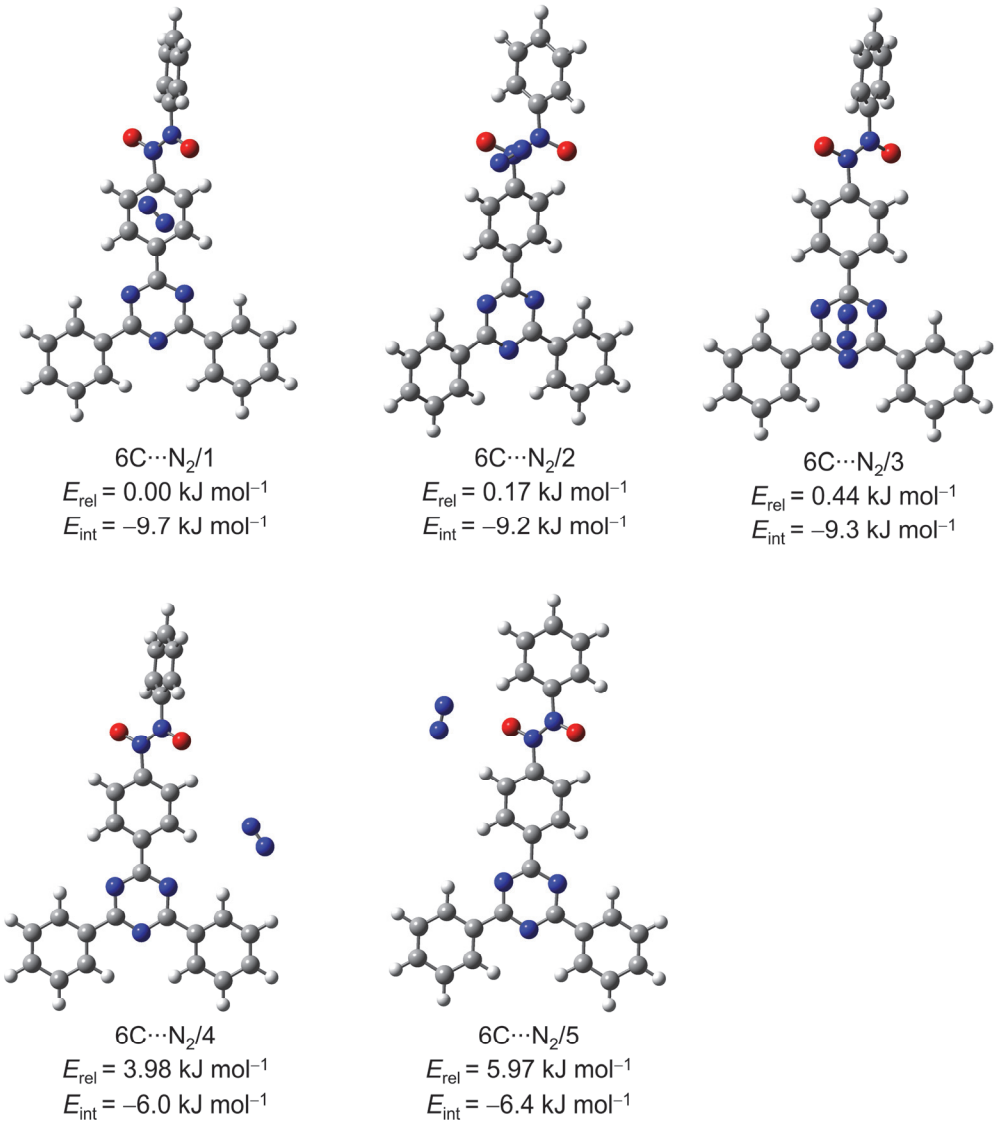

Figure S20. The B3LYP-D3(BJ)/def2-TZVP optimized geometries of the selected complexes between fragment **6C** and one molecule of N_2. Relative energies of the selected complexes (E_{rel}) and BSSE corrected interaction energies (E_{int}).

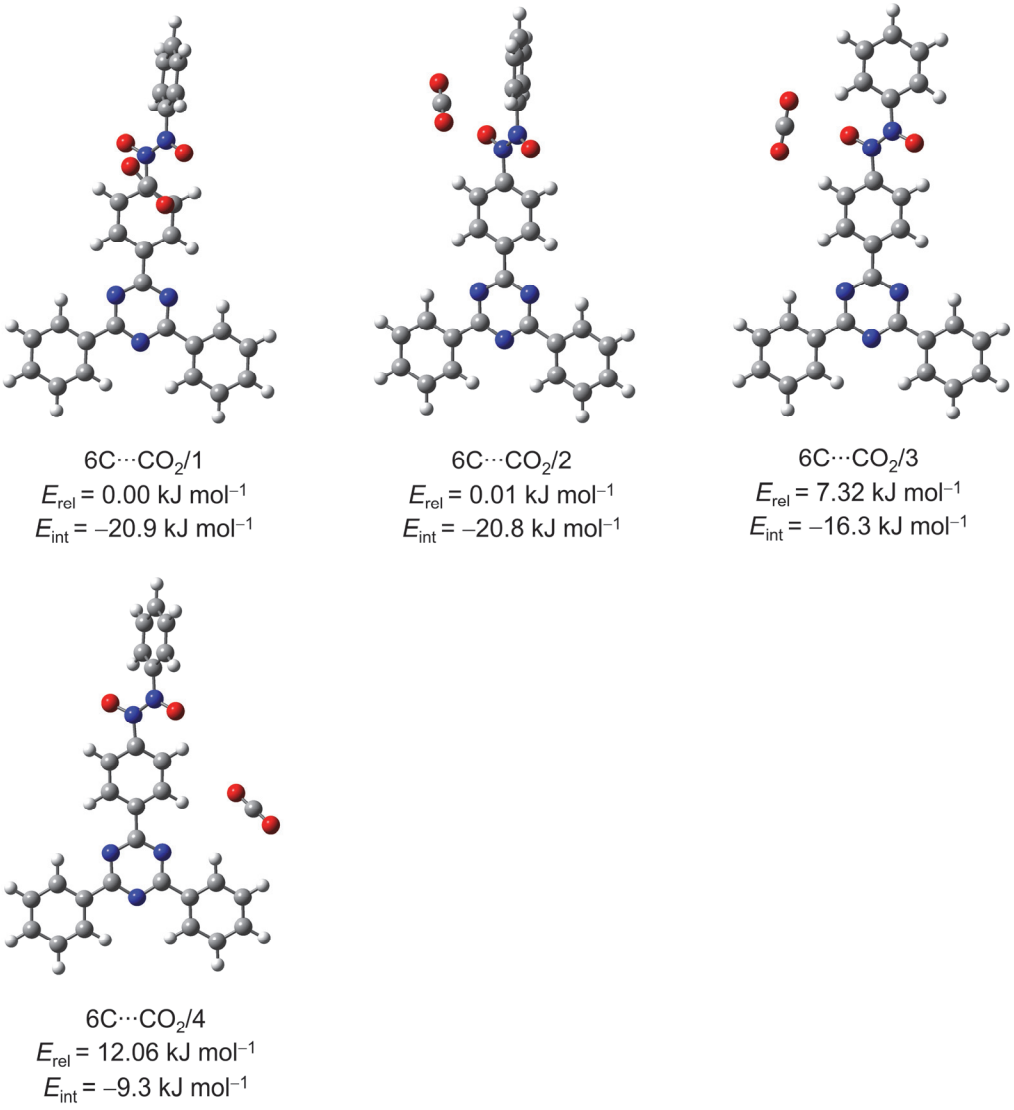

Figure S21. The B3LYP-D3(BJ)/def2-TZVP optimized geometries of the selected complexes between fragment **6C** and one molecule of CO_2. Relative energies of the selected complexes (E_{rel}) and BSSE corrected interaction energies (E_{int}).

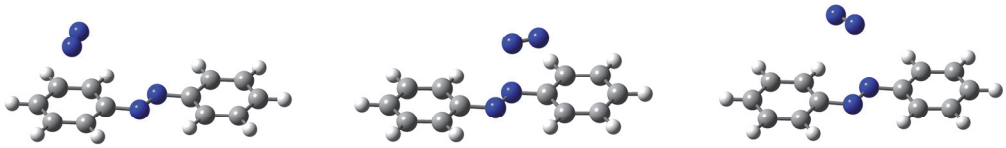

$D_{azo}\cdots N_2/1$
E_{rel} = 0.00 kJ mol^{-1}
E_{int} = –7.6 kJ mol^{-1}

$D_{azo}\cdots N_2/2$
E_{rel} = 0.59 kJ mol^{-1}
E_{int} = –7.0 kJ mol^{-1}

$D_{azo}\cdots N_2/3$
E_{rel} = 0.65 kJ mol^{-1}
E_{int} = –6.9 kJ mol^{-1}

Figure S22. The B3LYP-D3(BJ)/def2-TZVP optimized geometries of the selected complexes between fragment **D_{azo}** and one molecule of N_2. Relative energies of the selected complexes (E_{rel}) and BSSE corrected interaction energies (E_{int}).

$D_{azo}\cdots CO_2/1$
E_{rel} = 0.00 kJ mol^{-1}
E_{int} = –16.5 kJ mol^{-1}

$D_{azo}\cdots CO_2/2$
E_{rel} = 4.52 kJ mol^{-1}
E_{int} = –11.5 kJ mol^{-1}

Figure S23. The B3LYP-D3(BJ)/def2-TZVP optimized geometries of the selected complexes between fragment **D_{azo}** and one molecule of CO_2. Relative energies of the selected complexes (E_{rel}) and BSSE corrected interaction energies (E_{int}).

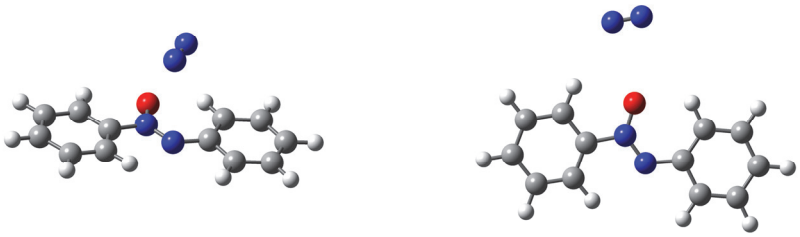

$D_{azoxy}\cdots N_2/1$
E_{rel} = 0.00 kJ mol^{-1}
E_{int} = –8.3 kJ mol^{-1}

$D_{azoxy}\cdots N_2/2$
E_{rel} = 3.28 kJ mol^{-1}
E_{int} = –5.48 kJ mol^{-1}

Figure S24. The B3LYP-D3(BJ)/def2-TZVP optimized geometries of the selected complexes between fragment **D_{azoxy}** and one molecule of N_2. Relative energies of the selected complexes (E_{rel}) and BSSE corrected interaction energies (E_{int}).

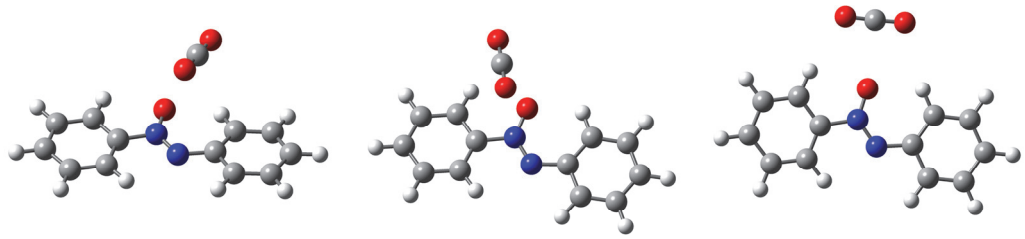

$D_{azoxy}\cdots CO_2/1$
E_{rel} = 0.00 kJ mol^{-1}
E_{int} = –17.7 kJ mol^{-1}

$D_{azoxy}\cdots CO_2/2$
E_{rel} = 1.86 kJ mol^{-1}
E_{int} = –15.7 kJ mol^{-1}

$D_{azoxy}\cdots CO_2/3$
E_{rel} = 2.75 kJ mol^{-1}
E_{int} = –15.1 kJ mol^{-1}

Figure S25. The B3LYP-D3(BJ)/def2-TZVP optimized geometries of the selected complexes between fragment **D_{azoxy}** and one molecule of CO_2. Relative energies of the selected complexes (E_{rel}) and BSSE corrected interaction energies (E_{int}).

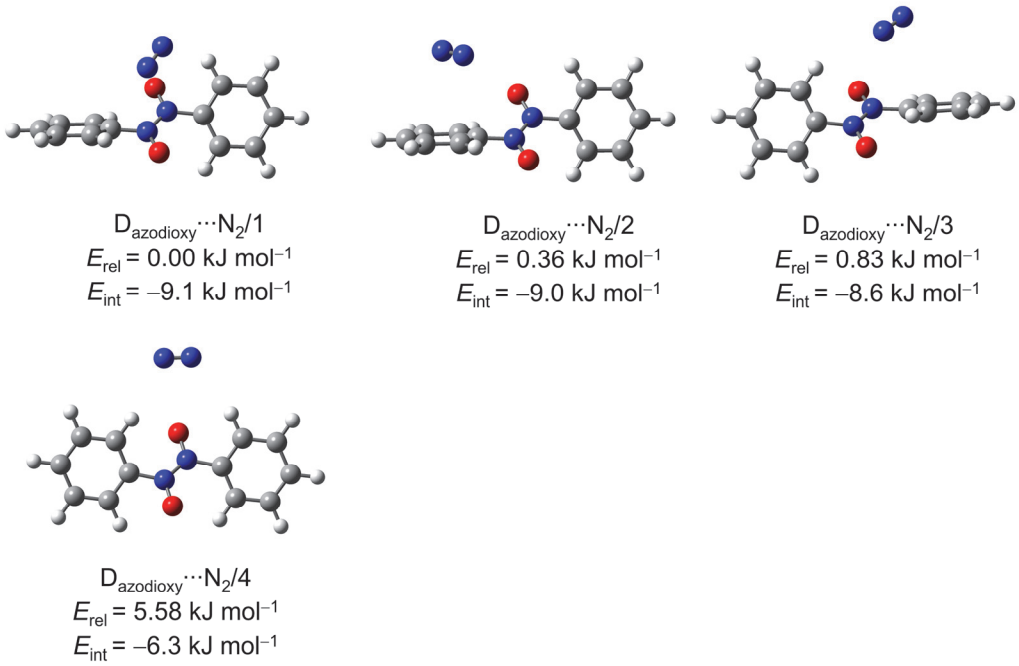

$D_{azodioxy}\cdots N_2/1$
E_{rel} = 0.00 kJ mol^{-1}
E_{int} = –9.1 kJ mol^{-1}

$D_{azodioxy}\cdots N_2/2$
E_{rel} = 0.36 kJ mol^{-1}
E_{int} = –9.0 kJ mol^{-1}

$D_{azodioxy}\cdots N_2/3$
E_{rel} = 0.83 kJ mol^{-1}
E_{int} = –8.6 kJ mol^{-1}

$D_{azodioxy}\cdots N_2/4$
E_{rel} = 5.58 kJ mol^{-1}
E_{int} = –6.3 kJ mol^{-1}

Figure S26. The B3LYP-D3(BJ)/def2-TZVP optimized geometries of the selected complexes between fragment **$D_{azodioxy}$** and one molecule of N_2. Relative energies of the selected complexes (E_{rel}) and BSSE corrected interaction energies (E_{int}).

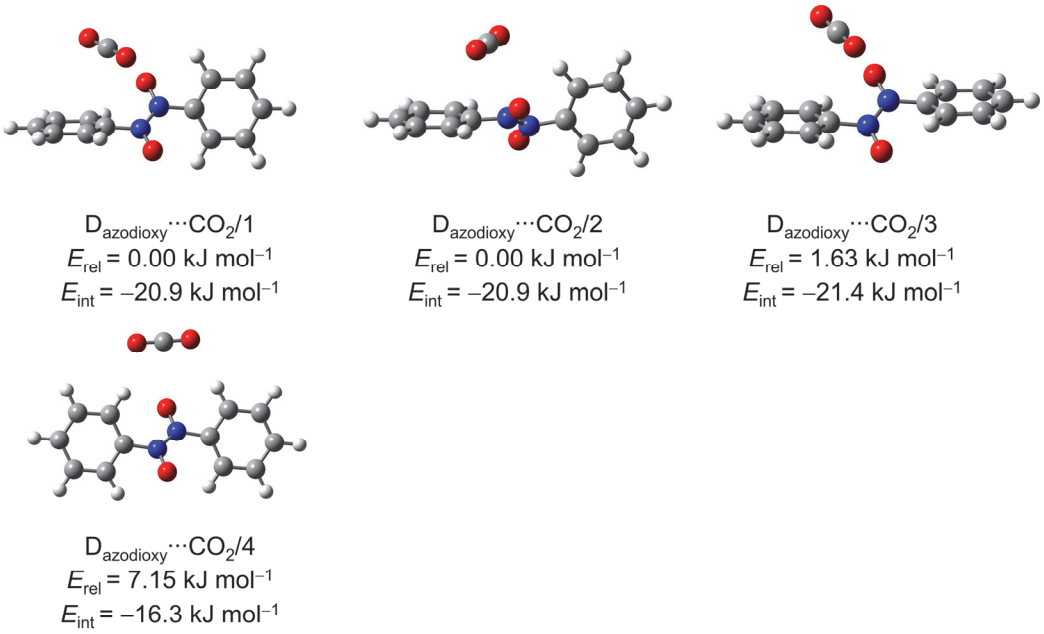

Figure S27. The B3LYP-D3(BJ)/def2-TZVP optimized geometries of the selected complexes between fragment **$D_{azodioxy}$** and one molecule of CO_2. Relative energies of the selected complexes (E_{rel}) and BSSE corrected interaction energies (E_{int}).

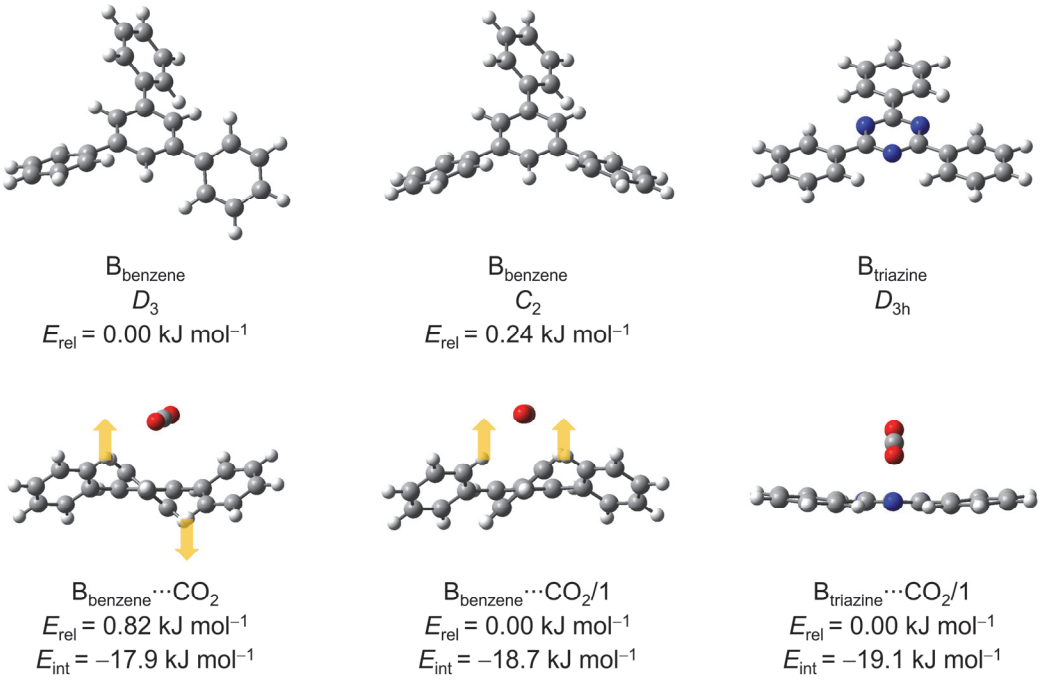

Figure S28. Different symmetries of **$B_{benzene}$** and **$B_{triazine}$**.

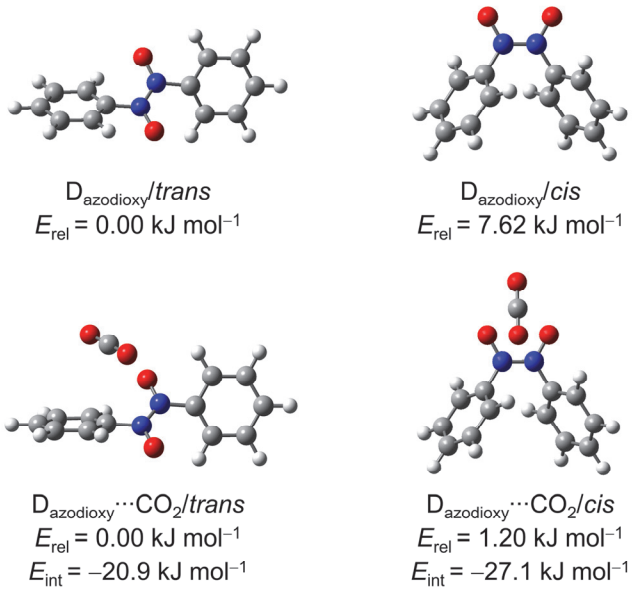

Figure S29. The B3LYP-D3(BJ)/def2-TZVP optimized geometries of the selected complexes between fragments **$D_{azodioxy}$/trans** and **$D_{azodioxy}$/cis** and one molecule of CO_2. Relative energies of the selected complexes (E_{rel}) and BSSE corrected interaction energies (E_{int}).

2. Model geometries for 2D layered structures

Table S1. Unit cell parameters (*a*, *b*, *c*, α, β and γ) of the optimized geometries of compounds **1–6** modeled as isolated 2D layers, AA, slipped AA' and AB stacked structures. The labels of the layer group (65) and space groups (143 and 147) used in the CRYSTAL17.

	Compound	Space group	CRYSTAL17 label	*a* / Å	*b* / Å	*c* / Å	α / °	β / °	γ / °
isolated 2D layers	1	*P* 3*	65	25.7201	25.7201				120
	2	*P* 3*	65	25.8038	25.8038				120
	3	*P* 3*	65	26.1164	26.1164				120
	4	*P* 3*	65	25.3792	25.3792				120
	5	*P* 3*	65	25.4422	25.4422				120
	6	*P* 3*	65	25.7271	25.7271				120
AA stacking	1	*P* $\bar{3}$	147	25.6247	25.6247	3.5830	90	90	120
	2	*P* 3	143	25.7786	25.7786	3.5784	90	90	120
	3	*P* $\bar{3}$	147	25.9885	25.9885	3.5542	90	90	120
	4	*P* $\bar{3}$	147	25.2081	25.2081	3.5170	90	90	120
	5	*P* 3	143	25.3362	25.3362	3.5125	90	90	120
	6	*P* $\bar{3}$	147	25.5813	25.5813	3.5051	90	90	120
AA' slipped	3	*P* $\bar{1}$	2	26.1926	25.3633	6.7752	108.0	82.6	118.2
AB stacking	1	*P* $\bar{3}$	147	25.7165	25.7165	6.4084	90	90	120
	2	*P* $\bar{3}$	147	25.7586	25.7586	6.3809	90	90	120
	3	*P* $\bar{3}$	147	26.0113	26.0113	6.3937	90	90	120
	4	*P* $\bar{3}$	147	25.3513	25.3513	6.0001	90	90	120
	5	*P* $\bar{3}$	147	25.4064	25.4064	5.9742	90	90	120
	6	*P* $\bar{3}$	147	25.4735	25.4735	5.9227	90	90	120

* the number of the corresponding space group, according to the Inernational Tables for Crystallography.

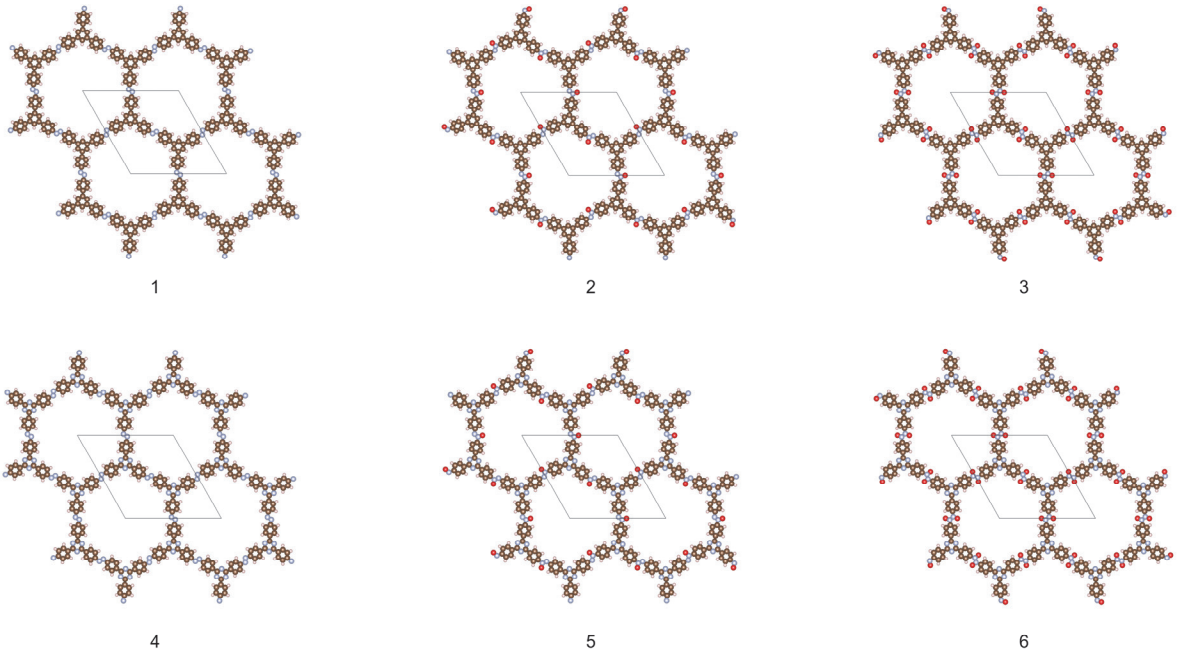

Figure S30. Schematic representation (along the c unit cell vector) of geometries (AA stacking) optimized at the PBE-D3/pob-TZVP-rev2 level of theory.

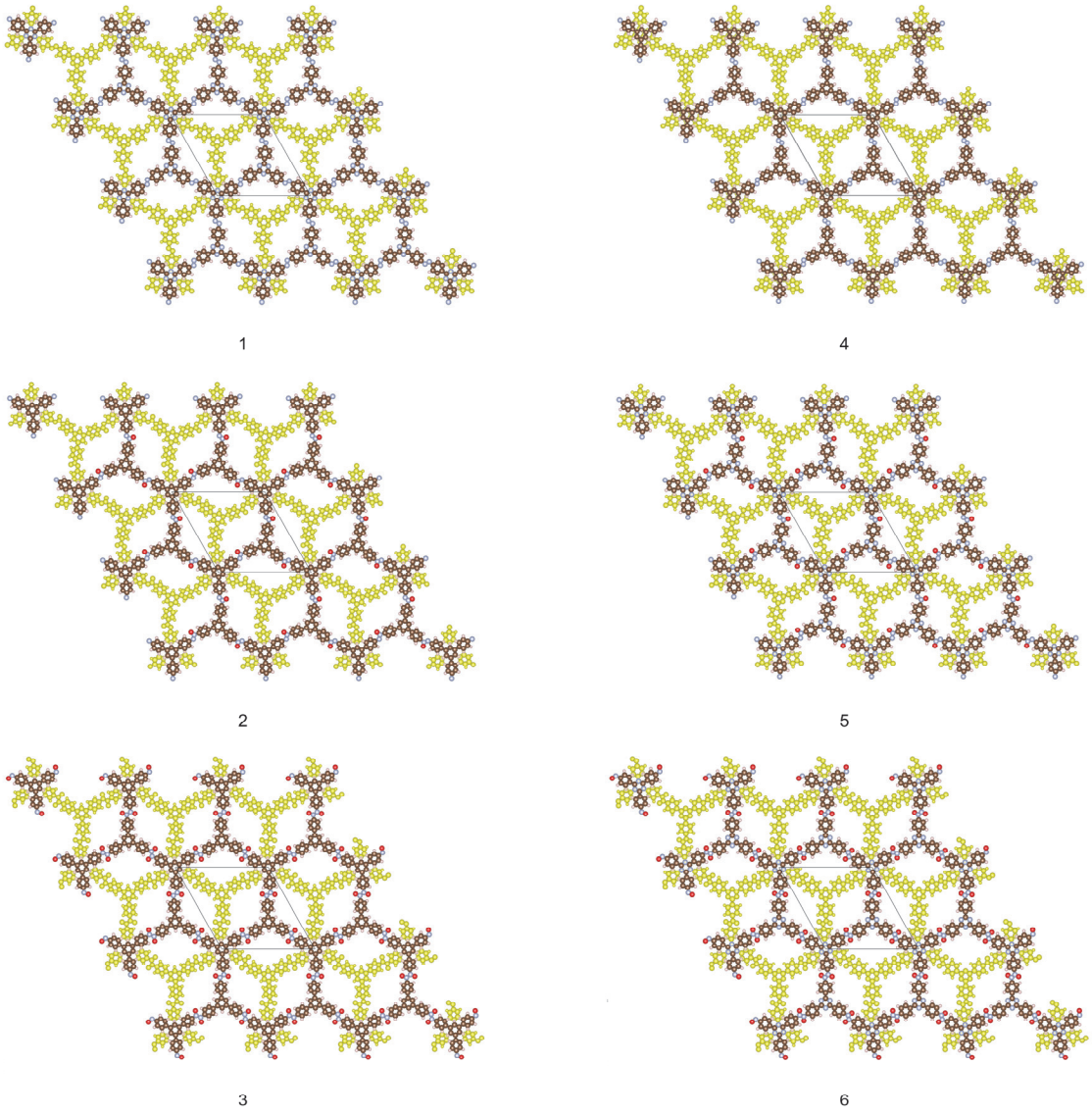

Figure S31. Schematic representation (along the c unit cell vector) of geometries (AB stacking) optimized at the PBE-D3/pob-TZVP-rev2 level of theory.

3. Electrostatic potential maps

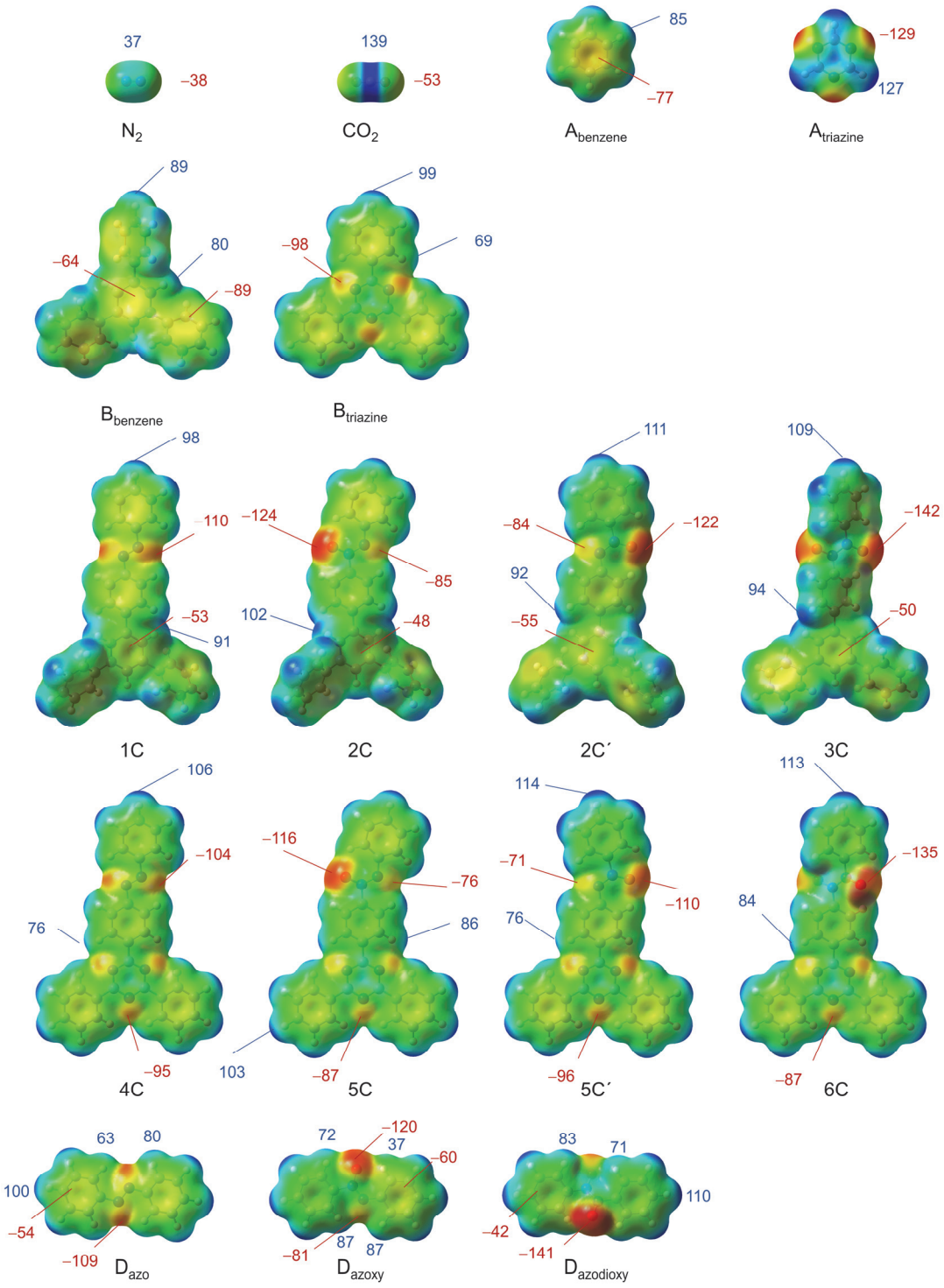

Figure S32. Electrostatic potential maps calculated at the PBE-D3/pob-TZVP-rev2 level of theory. ESP values (range from −142 kJ mol^{-1} e^{-1} to 151 kJ mol^{-1} e^{-1}) mapped on the 0.002 a.u. isodensity surface of selected molecules.

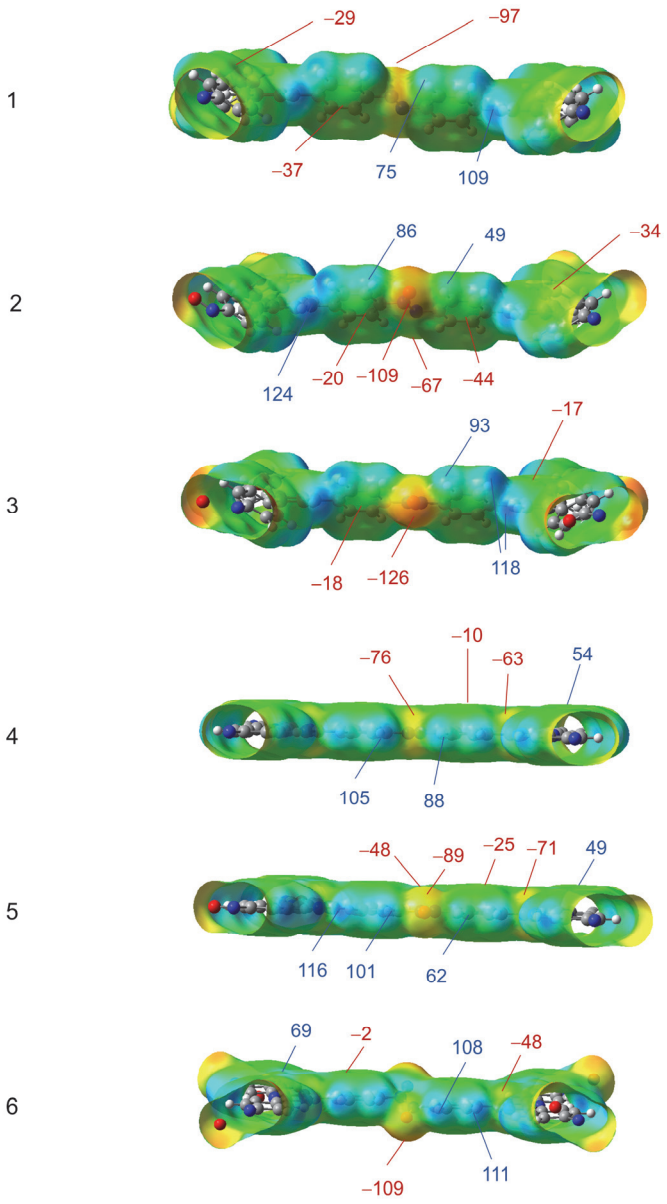

Figure S33. Electrostatic potential maps calculated at the PBE-D3/pob-TZVP-rev2 level of theory. ESP values (range from −142 kJ mol^{-1} to 151 kJ mol^{-1} e^{-1}) mapped on the 0.002 a.u. isodensity surface of isolated 2D layers represented with unit cells of compound **1–6.**

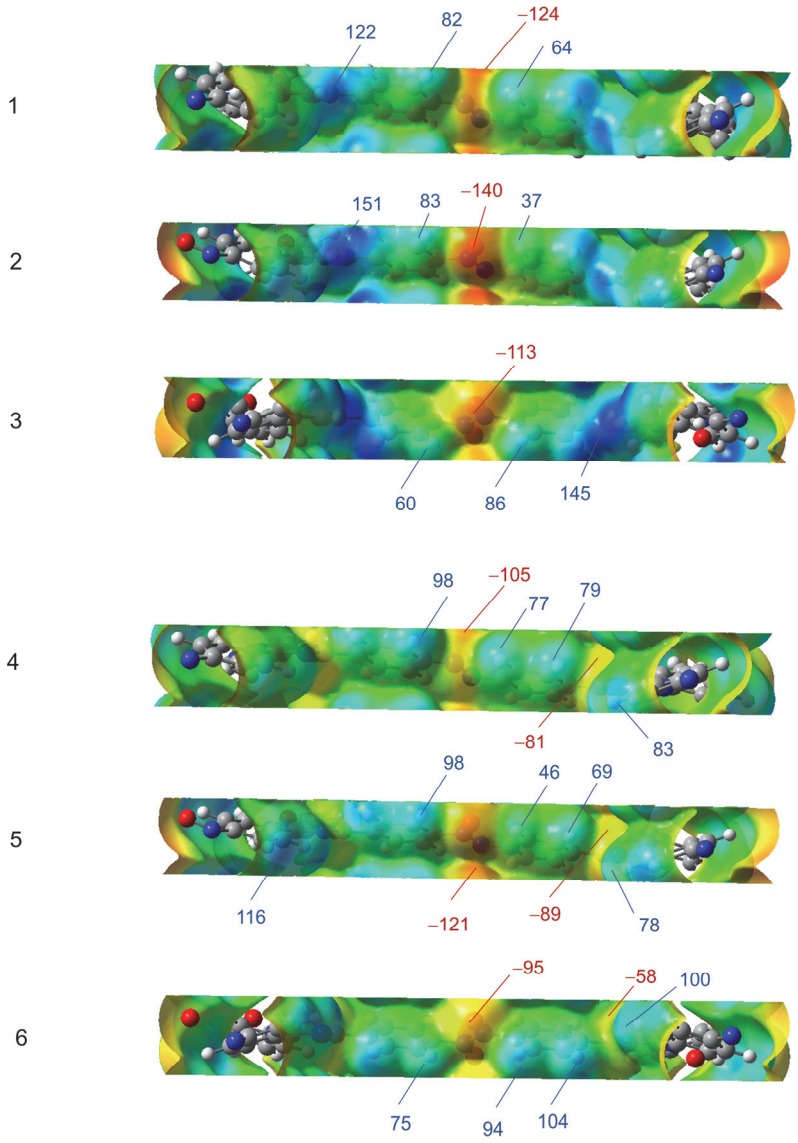

Figure S34. Electrostatic potential maps calculated at the PBE-D3/pob-TZVP-rev2 level of theory. ESP values (range from −142 kJ mol^{-1} to 151 kJ mol^{-1} e^{-1}) mapped on the 0.002 a.u. isodensity surface of AA stacked 2D layers represented with unit cells of compound **1**–**6**.

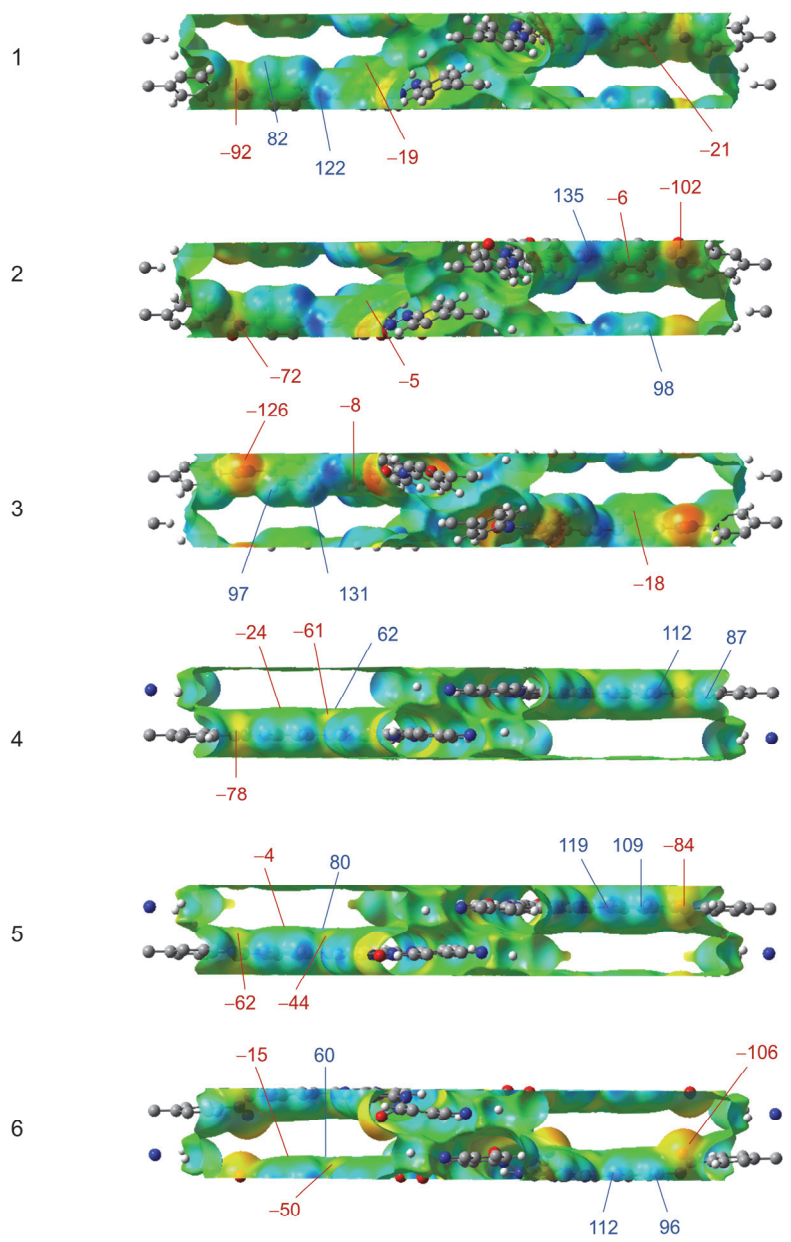

Figure S35. Electrostatic potential maps calculated at the PBE-D3/pob-TZVP-rev2 level of theory. ESP values (range from −142 kJ mol^{-1} to 151 kJ mol^{-1} e^{-1}) mapped on the 0.002 a.u. isodensity surface of AB stacked 2D layers represented with unit cells of compound **1**–**6**.

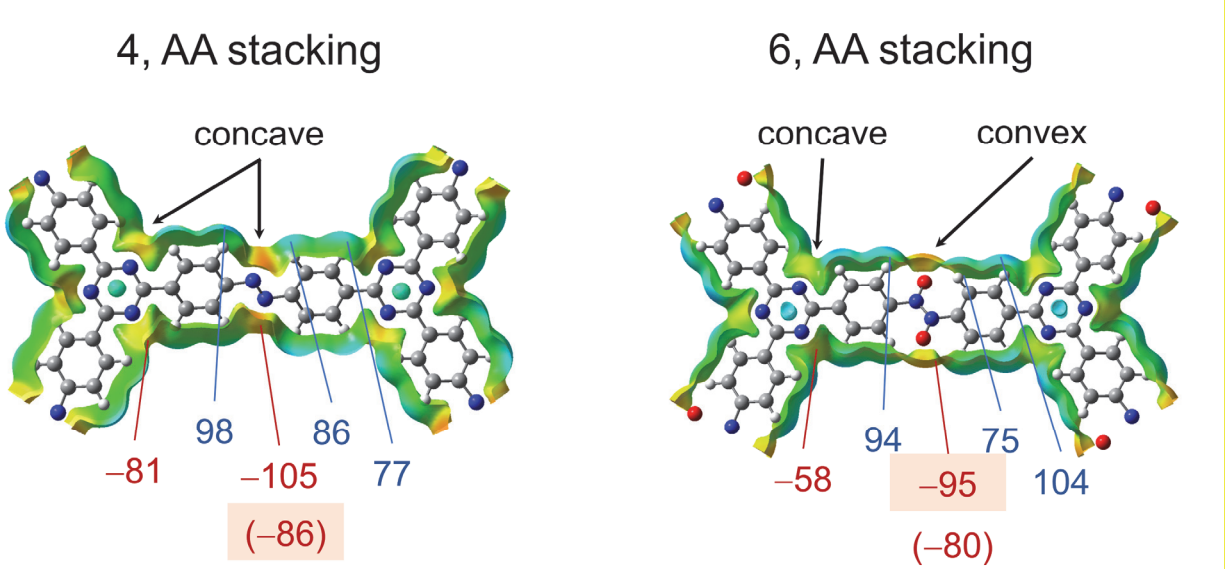

Figure S36. AA type of stacking of compounds **4** (azo) and **6** (azodioxy).

4. Adsorption isotherms and density plots

Table S2. Calculated framework properties of the AA, AA' slipped and AB stacked 2D layered compounds **1**–**6** (framework density, available pore volume and nitrogen surface area). The size of the simulation box used in the GCMC calculations.

	Compound	GCMC simulation box	Framework density, g/cm^3	Available pore volume, cm^3/g	Average surface area, m^2/g
AA stacking	1	2×2×8	0.563	1.140	1957
	2	2×2×8	0.596	1.069	1830
	3	2×2×8	0.628	1.012	1691
	4	2×2×8	0.598	1.031	1828
	5	2×2×8	0.633	0.965	1704
	6	2×2×8	0.663	0.928	1596
AA' slipped	3	2x2x4	0.693	0.863	1696
AB stacking	1	2×2×4	0.625	0.896	2462
	2	2×2×4	0.669	0.817	2284
	3	2×2×4	0.697	0.780	1949
	4	2×2×4	0.693	0.804	2411
	5	2×2×4	0.741	0.736	2077
	6	2×2×4	0.791	0.611	1636

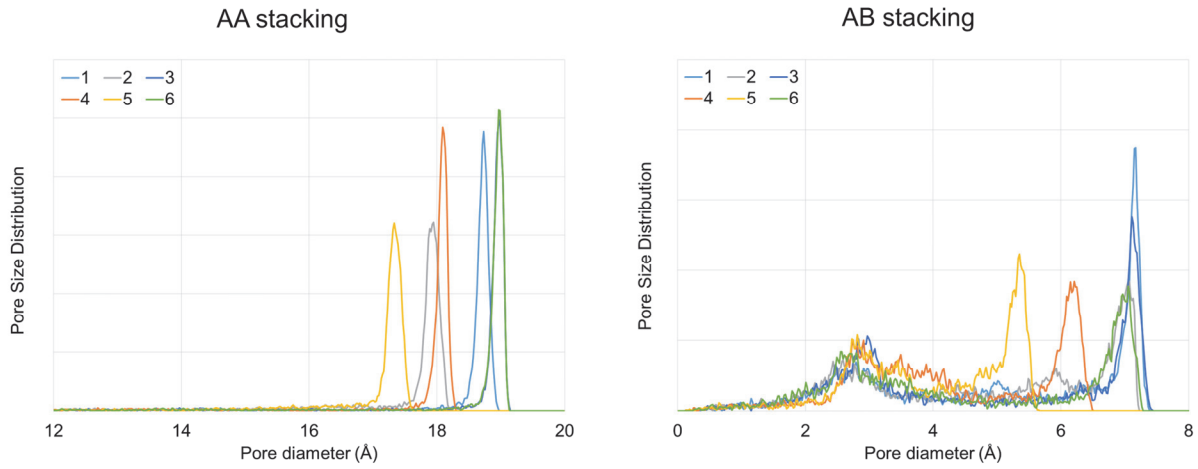

Figure S37. Pores size distribution of AA and AB stacked structures of **1**–**6**.

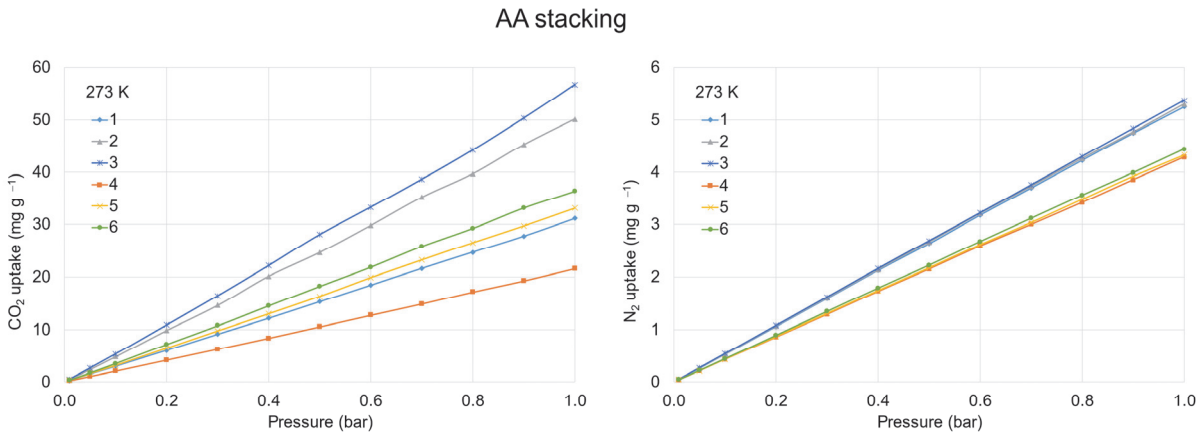

Figure S38. CO_2 and N_2 adsorption isotherms of AA stacked structures of **1**–**6** at 273 K.

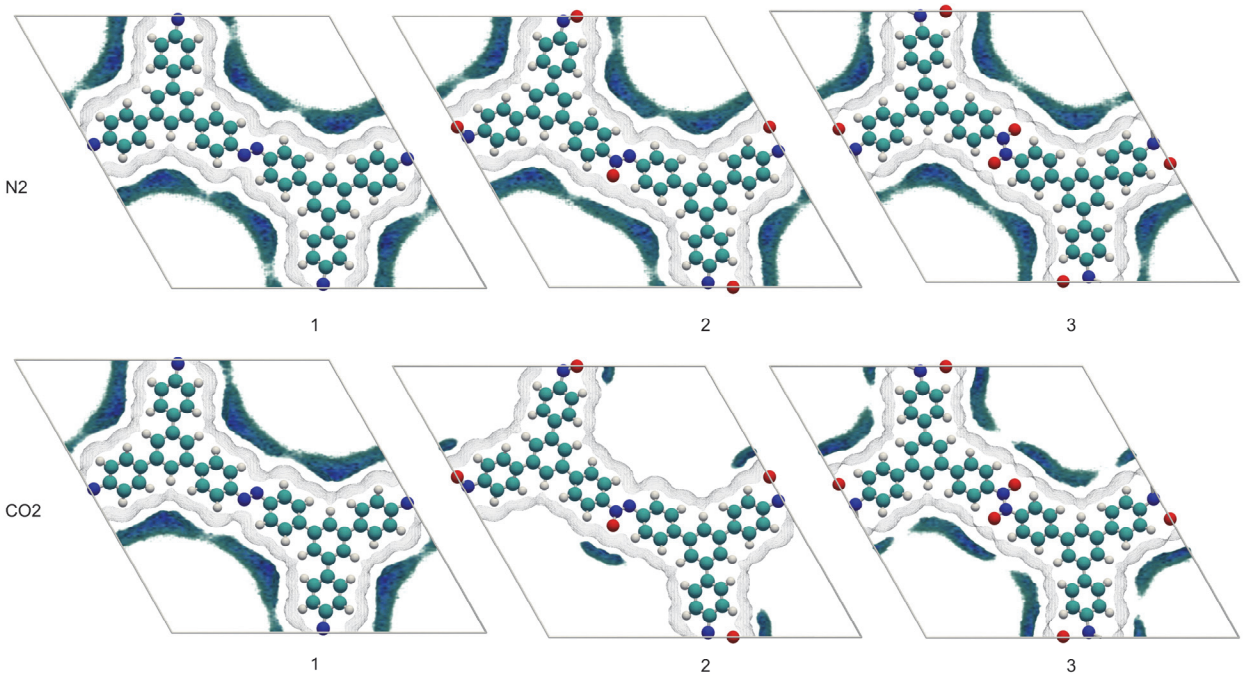

Figure S39. Density plots showing the average distribution of adsorbed N_2 and CO_2 molecules on AA stacked 2D layered frameworks of **1**–**3** at 298 K and 1 bar.

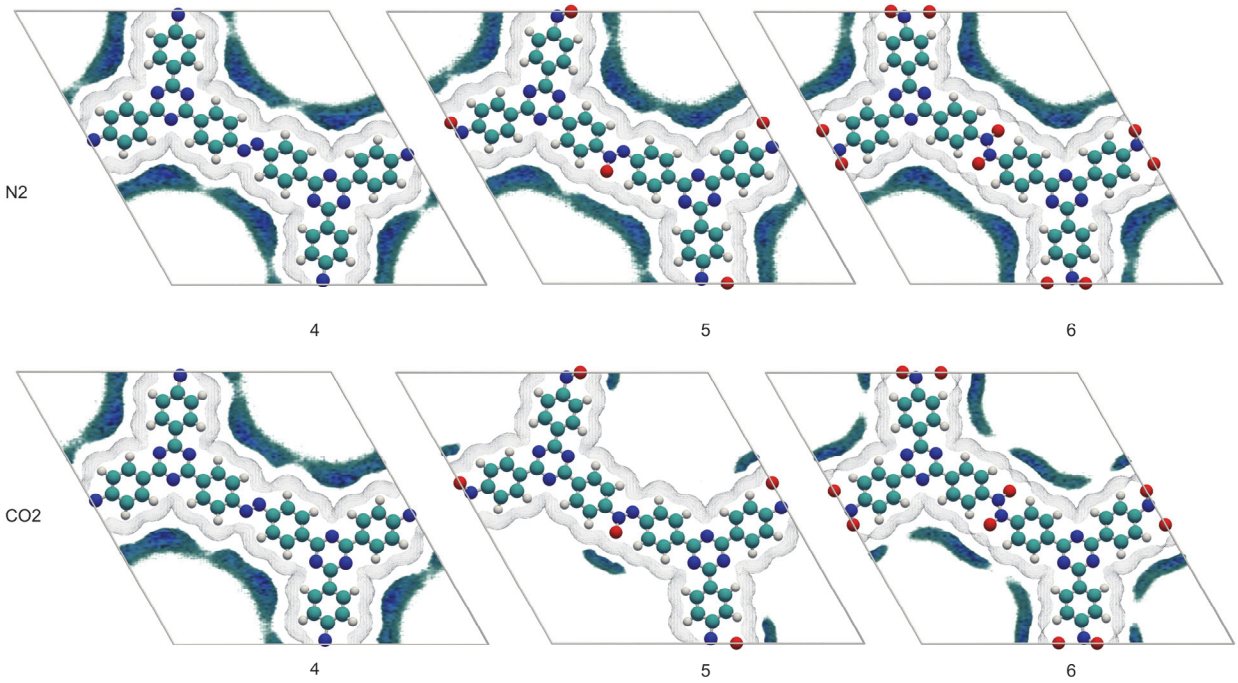

Figure S40. Density plots showing the average distribution of adsorbed N_2 and CO_2 molecules on AA stacked 2D layered frameworks of **4**–**6** at 298 K and 1 bar.

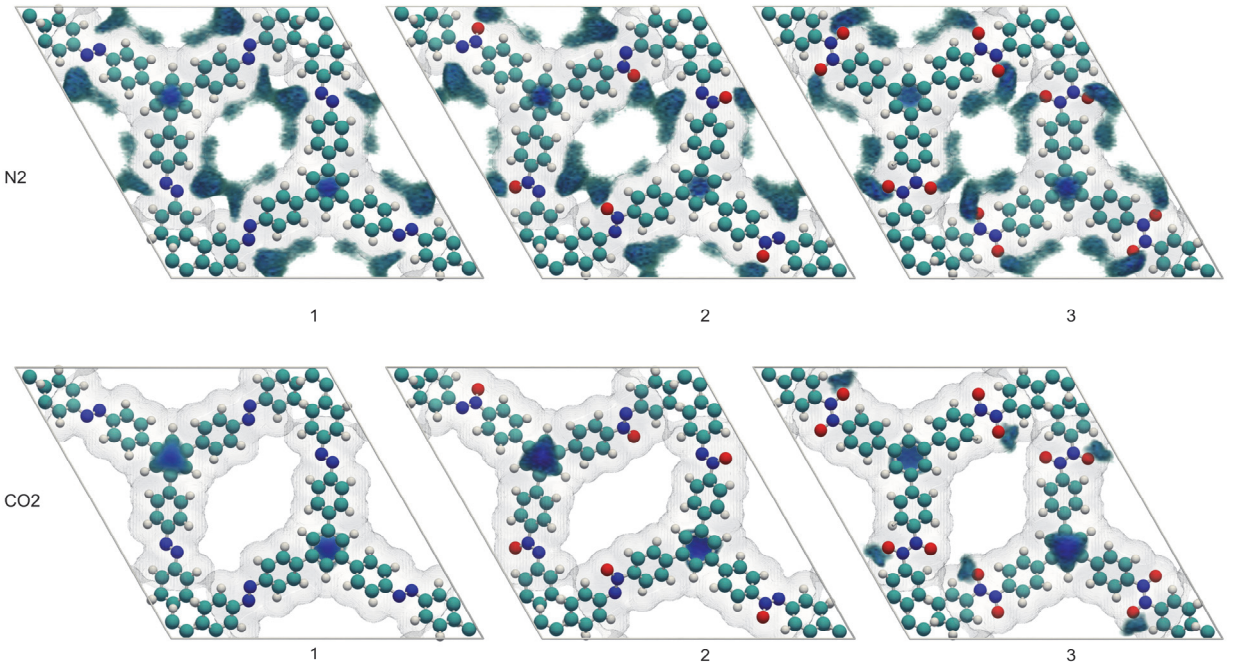

Figure S41. Density plots showing the average distribution of adsorbed N_2 and CO_2 molecules on AB stacked 2D layered frameworks of **1**–**3** at 298 K and 1 bar.

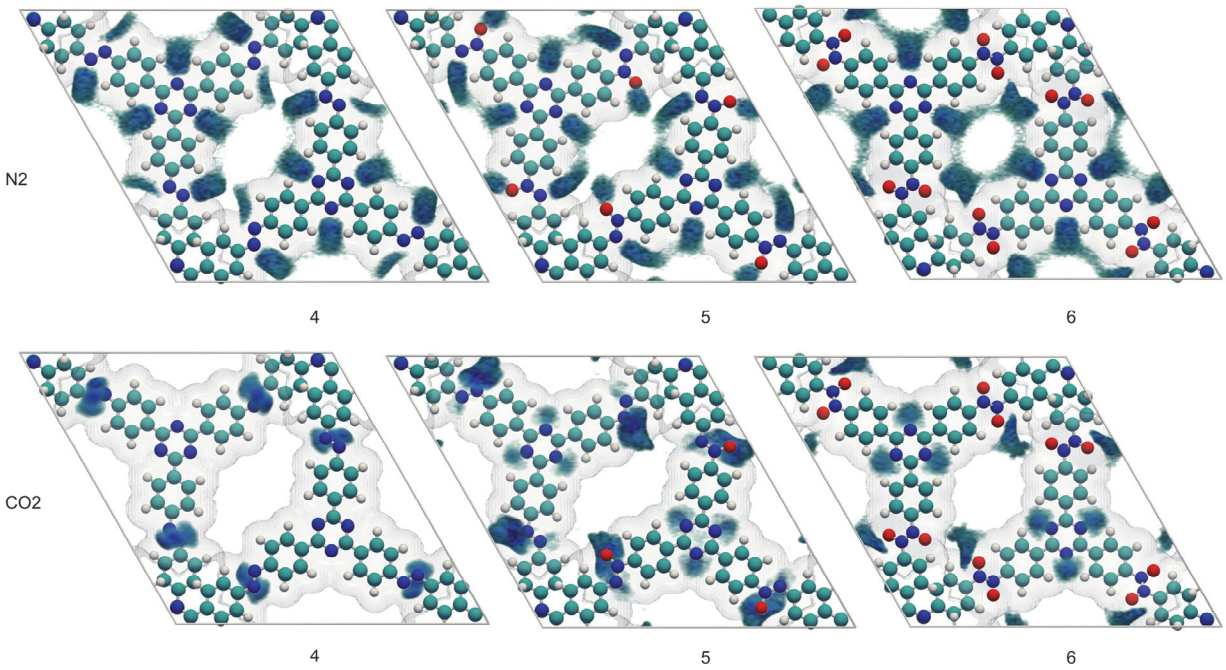

Figure S42. Density plots showing the average distribution of adsorbed N_2 and CO_2 molecules on AB stacked 2D layered frameworks of **4**–**6** at 298 K and 1 bar.

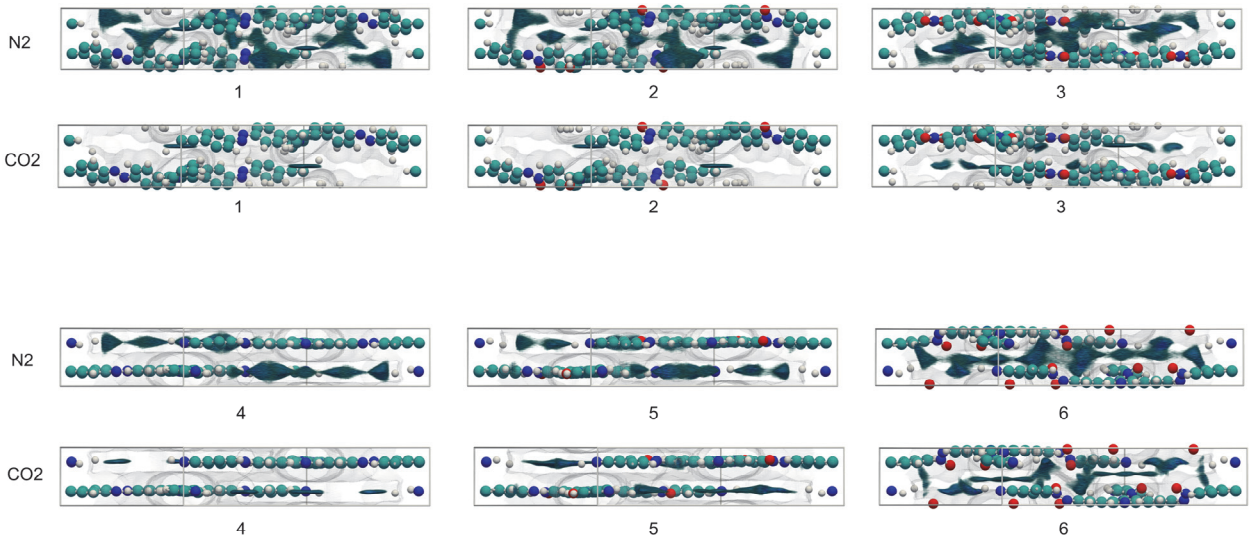

Figure S43. Density plots showing the average distribution of adsorbed N_2 and CO_2 molecules on AB stacked 2D layered frameworks of **1**–**6** at 298 K and 1 bar, side view.